

The proton–deuteron system in pionless EFT revisited

Sebastian König,^{1,2,*} Harald W. Griesshammer,^{3,4,†} and H.-W. Hammer^{5,6,2}

¹*Department of Physics, The Ohio State University, Columbus, Ohio 43210, USA*

²*Helmholtz-Institut für Strahlen- und Kernphysik (Theorie)
and Bethe Center for Theoretical Physics,
Universität Bonn, 53115 Bonn, Germany*

³*Institute for Nuclear Studies, Department of Physics,
George Washington University, Washington DC 20052, USA*

⁴*Forschungszentrum Jülich, D-52425 Jülich, Germany*

⁵*Institut für Kernphysik, Technische Universität Darmstadt, 64289 Darmstadt, Germany*

⁶*ExtreMe Matter Institute EMMI, GSI Helmholtzzentrum für
Schwerionenforschung GmbH, 64291 Darmstadt, Germany*

(Dated: January 22, 2015)

Abstract

We provide a detailed discussion of the low-energy proton–deuteron system in pionless effective field theory, considering both the spin-quartet and doublet S-wave channels. Extending and amending our previous work on the subject, we calculate the ${}^3\text{He}$ – ${}^3\text{H}$ binding energy difference both perturbatively (using properly normalized trinucleon wave functions) and non-perturbatively by resumming all $\mathcal{O}(\alpha)$ Coulomb diagrams in the doublet channel. Our nonperturbative result agrees well with a calculation that involves the full off-shell Coulomb T-matrix. Carefully examining the cutoff-dependence in the doublet channel, we present numerical evidence for a new three-nucleon counterterm being necessary at next-to-leading order if Coulomb effects are included. Indeed, such a term has recently been identified analytically. We furthermore make a case for a simplified Coulomb power counting that is consistent throughout the bound-state and scattering regimes. Finally, using a “partially screened” full off-shell Coulomb T-matrix, we investigate the importance of higher-order Coulomb corrections in low-energy quartet-channel scattering.

*Electronic address: koenig.389@physics.osu.edu

†Electronic address: hgrie@gwu.edu; permanent address: 3

I. INTRODUCTION

Effective field theories are powerful tools that can be used to carry out calculations in a formalism involving directly the relevant degrees of freedom for the physical system under consideration. In particular, in nuclear systems at very low energies and momenta, pion-exchange effects cannot be resolved and one can hence use the so-called *pionless effective field theory*. This approach only includes short-range contact interactions between nucleons [1–3] and is constructed to reproduce the effective range expansion [4] in the two-body system.

The applicability of this approach, which recovers Efimov’s universal approach to the three-nucleon problem [5, 6], stems from the experimental fact that the S-wave nucleon–nucleon scattering lengths in both the 3S_1 (isospin 0) channel, $a_d \approx 5.42$ fm, and in the 1S_0 (isospin 1) channel, $a_t \approx -23.71$ fm, are significantly larger than the range of interaction of about 1.4 fm set by the inverse pion mass. The corresponding effective ranges, on the other hand, have the values 1.75 and 2.73 fm, respectively, and are thus of the expected natural order of magnitude [7, 8]. In Refs. [9–14], the formalism has been extended to the three-nucleon sector. The situation there is particularly interesting because the triton can be interpreted as an approximate Efimov state. Recently, a fully perturbative calculation of neutron–deuteron scattering up to next-to-next-to-leading order has been carried out by J. Vanasse [15], using a novel technique that circumvents the (numerically expensive) calculation of full off-shell quantities.

Since most low-energy nuclear experiments involve more than one charged particle (proton), it is very important to discuss the treatment of Coulomb effects. Although this interaction can be treated as a perturbative correction for intermediate and higher energies, it becomes strong close to threshold and has to be treated nonperturbatively there. In the two-nucleon sector this was first discussed by Kong and Ravndal for the proton–proton channel [16, 17]. In Ref. [18], this analysis was extended to next-to-next-to-leading order. A renormalization-group analysis of proton–proton scattering in a distorted wave basis was carried out in Refs. [19, 20]. Moreover, the theory was applied to proton–proton fusion in Refs. [21, 22].

The three-nucleon sector with two charged particles was first discussed by Rupak and Kong in Ref. [23], who calculated Coulomb-modified scattering phase shifts for proton–deuteron scattering in the spin-quartet channel. A leading order calculation of the ^3He nucleus including nonperturbative Coulomb interactions has been carried out by Ando and Birse [24]. Including isospin breaking effects in the nucleon–nucleon scattering lengths, they obtained a good description of the ^3He – ^3H binding energy difference, but they did not consider scattering observables. A similar study at next-to-leading order in the pionless EFT was carried out using the resonating group method [25]. Those results do not include isospin breaking beyond^a Coulomb exchange and its associated contact interaction and are consistent with other determinations of the ^3He – ^3H binding energy difference.

The first calculation—within the framework of pionless EFT—of proton–deuteron scattering in the spin-doublet channel was presented by two of the present authors in Ref. [26]. The current paper, which is largely based on results from the first author’s doctoral thesis [27], extends—and in some aspects corrects—the earlier results (see in particular Sec. V A). After reviewing the formalism of pionless EFT in Secs II and III, we first focus on the bound-state sector. Using properly normalized trinucleon wave functions that are discussed in Sec. IV,

^a This crucial word is unfortunately missing in the journal version.

we calculate the ${}^3\text{He}$ – ${}^3\text{H}$ binding-energy difference in first-order perturbation theory, thereby correcting our earlier calculation presented in Ref. [26]. In the same section we then proceed and perform a nonperturbative determination of the ${}^3\text{He}$ binding energy. We find that the inclusion of the full off-shell Coulomb T-matrix as done by Ando and Birse [24] is clearly not necessary in the bound-state regime.

From the nonperturbative bound-state calculation we also find that the doublet-channel system beyond leading order does not seem to be renormalized correctly when Coulomb contributions are taken into account, a result that has recently been confirmed by analytical arguments [28].¹ We discuss our numerical findings in some detail in Section VI and also critically review the situation in the scattering regime, arguing to replace the Coulomb power counting introduced by Rupak and Kong [23] with a simpler scheme that simply includes all $\mathcal{O}(\alpha)$ Coulomb diagrams. This approach has the advantage of being consistent throughout the bound-state and scattering regimes. Finally, we investigate the importance of higher-order (in α) Coulomb effects in low-energy quartet-channel scattering in Sec. VII, before we close with a summary and an outlook. Some details about bound states in pionless EFT and the “partially-screened” Coulomb T-matrix used in Sec. VII are deferred to appendices.

II. FORMALISM AND BUILDING BLOCKS

We use the same formalism and notation as in Ref. [26], which we review here to make the present paper self-contained. The effective Lagrangian for the proton–deuteron system in pionless EFT can be written as

$$\begin{aligned} \mathcal{L} = & N^\dagger \left(iD_0 + \frac{\mathbf{D}^2}{2M_N} \right) N - d^{i\dagger} \left[\sigma_d + \left(iD_0 + \frac{\mathbf{D}^2}{4M_N} \right) \right] d^i - t^{A\dagger} \left[\sigma_t + \left(iD_0 + \frac{\mathbf{D}^2}{4M_N} \right) \right] t^A \\ & + y_d [d^{i\dagger} (N^T P_d^i N) + \text{h.c.}] + y_t [t^{A\dagger} (N^T P_t^A N) + \text{h.c.}] + \mathcal{L}_{\text{photon}} + \mathcal{L}_3, \quad (1) \end{aligned}$$

with the nucleon field N and two dibaryon fields d^i (with spin 1 and isospin 0) and t^A (with spin 0 and isospin 1), corresponding to the deuteron and the spin-singlet isospin-triplet virtual bound state in S-wave nucleon–nucleon scattering. The $y_{d,t}$ and $\sigma_{d,t}$ are two-body coupling constants that have to be fixed to experimental input data (see below). Both dibaryon fields are formally ghosts since their kinetic terms have a negative sign. This is required to reproduce the positive values of the effective ranges with short-range interactions [29]. Despite these “wrong” signs, the Lagrangian (1) can be shown to be equivalent to the most general version including only nucleon fields (see, for example, Ref. [30]). One can interpret the choice of signs in Eq. (1) as “avoiding” the Wigner bound [31–33], but since the effective N – N interactions (obtained by eliminating the dibaryon fields with the kinetic energy terms included) become energy-dependent, this is not a rigorous statement.

$M_N \approx 938.918$ MeV is the average nucleon mass. Although the proton–neutron mass difference is in part of electromagnetic origin, it is safe for us to neglect this kinematic effect

¹ We note here that the possibility of an α -dependent counterterm had already been discussed between HWH and U. van Kolck shortly after the publication of Ref. [26]; further discussions then took place between D. Phillips, SK, HWH, and HWG.

since $(M_p - M_n)/M_N \sim 0.005$ enters only at high orders in the EFT power counting.² For a more quantitative analysis, arguing that such corrections should be included at N³LO, see Ref. [34].

Spin and isospin degrees of freedom are included by treating the field N as a doublet in both spaces, but for notational convenience we usually suppress the spin and isospin indices of N . The operators

$$P_d^i = \frac{1}{\sqrt{8}} \sigma^2 \sigma^i \tau^2, \quad P_t^A = \frac{1}{\sqrt{8}} \sigma^2 \tau^2 \tau^A, \quad (2)$$

with the Pauli matrices $\vec{\sigma}$ and $\vec{\tau}$ operating in spin and isospin space, respectively, project out the 3S_1 and 1S_0 nucleon–nucleon partial waves. Note that for convenience we have written the effective Lagrangian (1) in isospin-symmetric form by considering only two distinct dibaryon fields. Alternatively, one could use states in the physical particle basis and consider different fields for the individual n - p , n - n , and p - p 1S_0 configurations. However, since the (inverse) scattering lengths and effective ranges in the n - n and n - p singlet channels are very similar, we do not need to distinguish these cases to the order we are working at in this paper. In the proton–proton sector, there is a significant breaking of isospin symmetry due to electromagnetic effects, so we will treat this subsystem separately (see Sec. II B below).

The covariant derivative

$$D_\mu = \partial_\mu + ieA_\mu \hat{Q}, \quad (3)$$

where \hat{Q} is the charge operator ($\hat{Q}_N = (\mathbf{1} + \tau_3)/2$, $\hat{Q}_d = \mathbf{1}$, ...), includes the coupling to the electromagnetic field. Furthermore, we have the kinetic and gauge fixing terms for the photons,

$$\mathcal{L}_{\text{photon}} = -\frac{1}{4} F_{\mu\nu} F^{\mu\nu} - \frac{1}{2\xi} (\partial_\mu A^\mu - \eta_\mu \eta_\nu \partial^\nu A^\mu)^2, \quad \eta_\mu = \text{timelike unit vector}, \quad (4)$$

of which we only keep contributions from Coulomb photons. These correspond to a static Coulomb potential between charged particles, but for convenience we introduce Feynman rules for a Coulomb-photon propagator,

$$\Delta_{\text{Coulomb}}(k) = \frac{i}{\mathbf{k}^2 + \lambda^2}, \quad (5)$$

which we draw as a wavy line, and factors $(\pm ie \hat{Q})$ for the vertices.³ Following Ref. [23], we have regulated the singularity of the Coulomb-photon propagator at zero momentum transfer by introducing a photon mass λ in Eq. (5). This corresponds to a screening of the Coulomb interaction in configuration space by writing it as a Yukawa potential $\sim e^{-\lambda r}/r$. In the numerical calculations that will be discussed later on, λ is always taken to be small (typically well below 1 MeV). In fact, by choosing a mesh-point distribution dense around the Coulomb peak it is possible to numerically take the zero-screening limit $\lambda \rightarrow 0$ [26].

S-wave nucleon–deuteron scattering can take place in either a spin- $3/2$ (quartet channel) or spin- $1/2$ (doublet channel) configuration. In the doublet channel, a three-body contact

² For example, in a neutron propagator with momentum k one would have $k^2/(2M_n) = k^2/(2M_N + \Delta M_N) = k^2/(2M_N) \times [1 - \Delta M_N/(2M_N) + \dots]$ with $\Delta M_N = M_n - M_p$.

³ Due to the sign convention chosen in the Lagrangian (1), dibaryon–photon vertices get an additional minus sign.

interaction is required for renormalization already at leading order in the EFT [11]. We write it here as in Refs. [24, 35] as

$$\mathcal{L}_3 = \frac{M_N H(\Lambda)}{3\Lambda^2} N^\dagger \left(y_d^2 (d^i)^\dagger d^j \sigma^i \sigma^j + y_t^2 (t^A)^\dagger t^B \tau^A \tau^B - y_d y_t [(d^i)^\dagger t^A \sigma^i \tau^A + \text{h.c.}] \right) N, \quad (6)$$

where Λ is a momentum cutoff applied in the three-body equations discussed below and $H(\Lambda)$ a known log-periodic function of the cutoff that depends on a three-body parameter Λ_* .

A. Full dibaryon propagators

It is a well-known feature of pionless EFT that according to the standard power counting for systems with large S-wave scattering lengths [1, 2] the bare dibaryon propagators have to be dressed by nucleon bubbles to all orders in order to get the full leading-order expressions. The resulting geometric series are shown in Fig. 1.

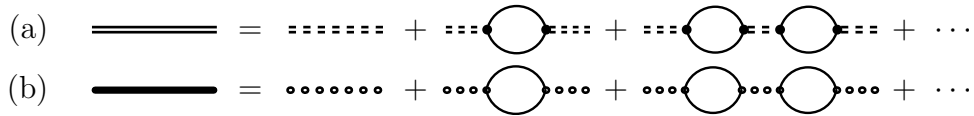


FIG. 1: Full dibaryon propagators in (a) the 3S_1 state (*i.e.*, the deuteron) and (b) the 1S_0 state.

For convenience, we also resum the effective range corrections that arise when the dibaryons in the theory are promoted to dynamical fields by including their kinetic terms. We do not go into the details of the calculations here and simply quote the results for the renormalized propagators. They are obtained by demanding that the (S-wave) effective range expansions

$$k \cot \delta_d = -\gamma_d + \frac{\rho_d}{2}(k^2 + \gamma_d^2) + \dots \quad (7)$$

around the deuteron pole⁴ at $k = i\gamma_d = i\sqrt{M_N E_d}$, and

$$k \cot \delta_t = -\frac{1}{a_t} + \frac{\rho_t}{2}k^2 + \dots \quad (8)$$

for the singlet channel are reproduced. The expansion for the singlet channel is around zero momentum; alternatively one could also expand here around the position of the virtual bound state. In writing Eq. (8), however, we have used that $\rho_t = r_{0t}$ to the order we are working at and will in the following also identify $\gamma_t \equiv 1/a_t$ to make the notation more symmetric. After renormalization in the PDS scheme [36], the fully resummed propagators are

$$\Delta_d^{ij}(p) \equiv \delta^{ij} \Delta_d(p) = -\frac{4\pi i}{M_N y_d^2} \cdot \frac{\delta^{ij}}{-\gamma_d + \sqrt{\frac{\mathbf{p}^2}{4} - M_N p_0 - i\varepsilon - \frac{\rho_d}{2} \left(\frac{\mathbf{p}^2}{4} - M_N p_0 - \gamma_d^2 \right)}} \quad (9)$$

⁴ The notation ρ_d is used in the quadratic term of Eq. (7) because the expansion is not around zero momentum. The difference of ρ_d to the effective range in a standard expansion around zero momentum is smaller than 1% [7].

and

$$\Delta_t^{AB}(p) \equiv \delta^{AB} \Delta_t(p) = -\frac{4\pi i}{M_N y_t^2} \cdot \frac{\delta^{AB}}{-\gamma_t + \sqrt{\frac{\mathbf{p}^2}{4} - M_N p_0 - i\varepsilon} - \frac{\rho_t}{2} \left(\frac{\mathbf{p}^2}{4} - M_N p_0 \right)}, \quad (10)$$

which means that we have fixed the parameters appearing in the effective Lagrangian according to

$$\sigma_{d,t} = \frac{2}{M_N} \frac{\mu - \gamma_{d,t}}{\rho_{d,t}}, \quad y_{d,t}^2 = \frac{8\pi}{M_N^2} \frac{1}{\rho_{d,t}}, \quad (11)$$

where μ is the PDS renormalization scale. These expressions are valid up to N²LO since the resummation of the effective-range contributions only includes a subset of higher-order (N³LO etc.) terms. At leading order, range corrections are not included and the dibaryon kinetic terms do not contribute. The corresponding propagators are obtained by setting $\rho_t = 0$ and $\rho_d = 0$ in Eqs. (9) and (10), while perturbative expressions for the NLO and N²LO propagators can be obtained by expanding the equations up to linear and quadratic order in ρ_d and ρ_t , respectively. For example, one finds

$$\begin{aligned} \Delta_d(p) = & -\frac{4\pi}{M_N y_d^2} \cdot \frac{1}{-\gamma_d + \sqrt{\frac{\mathbf{p}^2}{4} - M_N p_0 - i\varepsilon}} \\ & \times \left[1 + \frac{\rho_d}{2} \frac{\mathbf{p}^2/4 - M_N p_0 - \gamma_d^2}{-\gamma_d + \sqrt{\frac{\mathbf{p}^2}{4} - M_N p_0 - i\varepsilon}} + \left(\frac{\rho_d}{2} \frac{\mathbf{p}^2/4 - M_N p_0 - \gamma_d^2}{-\gamma_d + \sqrt{\frac{\mathbf{p}^2}{4} - M_N p_0 - i\varepsilon}} \right)^2 + \dots \right]. \quad (12) \end{aligned}$$

Using these propagators then in the three-body equations (see below) amounts to a ‘‘partial resummation’’ of effective-range corrections [14]. For each expression, the corresponding deuteron wave function renormalization constant is given by the residue at the bound state pole:

$$Z_0^{-1} = i \frac{\partial}{\partial p_0} \frac{1}{\Delta_d(p)} \Big|_{p_0 = -\frac{\gamma_d^2}{M_N}, \mathbf{p}=0}. \quad (13)$$

At leading order, one simply has

$$Z_0^{\text{LO}} = \gamma_d \rho_d, \quad (14)$$

whereas the result from the fully resummed expression (9) is

$$Z_0^{\text{N}^2\text{LO}} = \frac{\gamma_d \rho_d}{1 - \gamma_d \rho_d}. \quad (15)$$

The expressions for the perturbatively expanded propagators can then simply be read off from the geometric series

$$\frac{1}{1 - \gamma_d \rho_d} = 1 + \gamma_d \rho_d + (\gamma_d \rho_d)^2 + \dots. \quad (16)$$

Note that since $\gamma_d \rho_d \approx 0.4$, the above series converges only rather slowly. This fact can be taken into account by choosing an alternative renormalization scheme, called *Z-parametrization* [37], that is constructed in such a way that it produces the fully resummed Z_0 as given in Eq. (15) already at NLO. In Ref. [38] the approach has been applied to the

three-nucleon system in pionless EFT and shown to improve the overall convergence of the theory. In the present work, however, where as in Ref. [26] we are primarily interested in the inclusion of Coulomb effects, we use the simpler scheme with the propagators as given in Eqs. (9) and (10).

Furthermore we point out that, as mentioned in Ref. [14], the partial resummation of higher-order corrections in the propagators is made for convenience only and does certainly not improve the accuracy of the calculation. We will discuss below that in fact it may introduce uncontrolled effects by modifying the ultraviolet behavior of the half off-shell amplitudes. In the future it will be advisable to only perform calculations that treat effective-range corrections strictly perturbatively. For the three-boson system this procedure has been carried out up to N²LO by Ji and Phillips in Ref. [39]. Recently, an analogous calculation for the neutron–deuteron system has been presented in Ref. [15], using a new approach that greatly reduces the computational cost by not requiring to determine the full off-shell scattering amplitude. The approach can be adapted to also include Coulomb effects [40].

B. Coulomb contributions in the proton–proton system

The Coulomb interaction breaks the isospin symmetry that is implicit in the dibaryon propagators considered so far. For the p – p part of the singlet dibaryon we can also have Coulomb-photon exchanges inside the nucleon bubble. These can be resummed to all orders, yielding a dressed nucleon bubble [16, 17] that is subsequently used to calculate the full singlet-dibaryon propagator in the p – p channel. This is shown in Fig. 2. The result for the leading order propagator is [24]

$$\Delta_{t,pp}^{AB}(p) \equiv \delta^{AB} \Delta_{t,pp}(p) = -\frac{4\pi i}{M_N y_t^2} \cdot \frac{\delta^{AB}}{-1/a_C - \gamma \tilde{h}_0(p')} \quad (17)$$

with

$$\gamma = \gamma_{p-p} = \alpha M_N \quad , \quad \alpha = \frac{e^2}{4\pi} \approx \frac{1}{137} \quad , \quad p' = i\sqrt{\mathbf{p}^2/4 - M_N p_0 - i\varepsilon} \quad , \quad (18)$$

and Euler’s digamma function $\psi(x)$ in

$$\tilde{h}_0(p') = \psi(i\eta) + \frac{1}{2i\eta} - \log(i\eta) \quad , \quad \eta = \eta(p') = \frac{\gamma}{2p'} \quad . \quad (19)$$

This means that the Coulomb-modified effective range expansion⁵ has been used for renormalization. Note that since the matching is done to observables, this procedure is model-independent and simultaneously takes into account strong and electromagnetic isospin-breaking effects, which are not separated.

We denote here the p – p S-wave scattering length simply as a_C . Corrections due to the corresponding Coulomb-modified effective range r_C can be included in the same way as described in the preceding section by first resumming insertions of the kinetic-energy operators to all orders and then matching the result to reproduce the modified effective range expansion up to quadratic order.

⁵ See, for example, Ref. [41] and references therein.

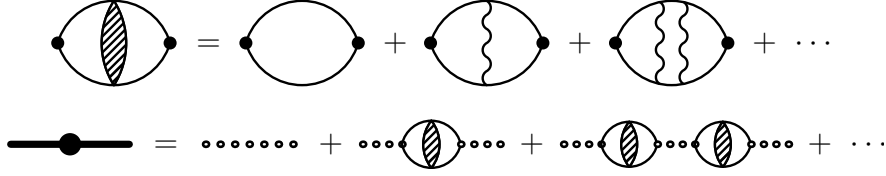


FIG. 2: Dressed nucleon bubble and full singlet dibaryon propagator in the p - p channel.

To simplify the equations that we give later on, we introduce here the propagator functions

$$D_{d,t}(E; q) \equiv (-i) \cdot \Delta_{d,t} \left(E - \frac{q^2}{2M_N}, q \right) \quad (20)$$

and

$$D_t^{pp}(E; q) \equiv (-i) \cdot \Delta_{t,pp} \left(E - \frac{q^2}{2M_N}, q \right). \quad (21)$$

C. Power counting

1. Strong sector

Without electromagnetic effects, one can apply the standard power counting for pionless EFT that has been extensively discussed in the literature (see the reviews [8, 42, 43] and references therein). In this case, the typical low-energy scale Q of the theory is set by the deuteron binding momentum $\gamma_d \approx 45$ MeV. We can formally count the external momenta k, p to be of the same order. Since we are working in a setup without explicit pions, the natural breakdown scale of our theory is of the order of the pion mass, $\Lambda_{\not{\pi}} \sim M_{\pi}$. The combination of the two scales yields the expansion parameter $Q/\Lambda_{\not{\pi}} \sim 1/3$ of pionless EFT.

In the three-body sector, one finds that the one-nucleon-exchange interaction (see *e.g.* Fig. 4) has to be iterated to all orders in order to get the neutron–deuteron scattering amplitude (or T-matrix). As will be discussed in more detail in the following section, this procedure yields integral equations in momentum space that can be solved numerically with an explicit ultraviolet cutoff Λ , which has to be chosen at least as large as $\Lambda_{\not{\pi}}$ in order to capture all low-energy physics. This is thus the scale we use below to estimate loop contributions.

We will use variations of the numerical cutoff Λ to assess the numerical uncertainty and convergence of our calculation. We stress here, however, that this gives typically only a lower bound on the true uncertainty of our results, which is determined, at any given order, by powers of the EFT expansion parameter $Q/\Lambda_{\not{\pi}}$.

2. Including Coulomb effects

The power counting has to be amended in order to incorporate Coulomb effects. For the p - d system this was first done by Rupak and Kong in Ref. [23]. From the form of the (Yukawa-screened) Coulomb potential in momentum space,

$$V_{c,\lambda}(q) \sim \frac{\alpha}{q^2 + \lambda^2}, \quad (22)$$

it is clear that Coulomb contributions dominate for small momentum transfers. As noted in Ref. [23], they enter $\sim \alpha M_N/q$, *i.e.*, proportional to the Coulomb parameter η ; *cf.* Eq. (19). This behavior is not captured by the power counting for the strong sector, which consequently has to be modified in order to perform calculations including Coulomb effects for small external momenta.

Most importantly, one can no longer simply assume that the scale of all momenta is set by the deuteron binding momentum, $Q \sim \gamma_d$. Instead, one has to keep track of the new scale introduced by the external momenta separately. Rupak and Kong [23] generically denote this scale by p and assume $p \ll Q$ for the power counting, meaning that one makes a simultaneous expansion in *two* small parameters Q/Λ_π and $p/(\alpha M_N)$ [23].⁶

Deducing the scaling of loops in this scheme is not straightforward anymore. In fact, the whole discussion (see Ref. [26] and the original Ref. [23]) becomes quite cumbersome. In the following, we present the bottom line and will present a simpler approach in Sec. VI E that has the advantage of being consistent throughout the scattering and bound-state regimes.

3. Selected diagrams

In Fig. 3 we show all diagrams contributing to p - d scattering that involve a single Coulomb-photon exchange and are thus of order α . The last one, diagram (d) has the most straightforward behavior since it simply scales as α/p^2 . Diagram (a) has the same factor because also here the Coulomb-photon propagator involves the external momentum scale p , but it is further enhanced by a factor Λ_π/Q from the nucleon bubble, which is easy to count as there are no Coulomb-photon exchanges inside the bubble. This is of course in perfect agreement with the fact that the direct coupling of the photon to the dibaryon—generated by gauging the dibaryon kinetic energy operators—only enters at NLO in the EFT counting. This makes diagram (d) both $\mathcal{O}(\alpha)$ *and* an effective-range correction $\sim \rho_{d,t}$.

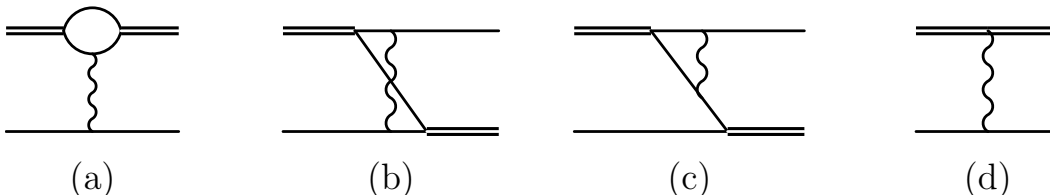


FIG. 3: Leading $\mathcal{O}(\alpha)$ diagrams involving Coulomb photons.

In both diagrams (b) and (c) the loops do not involve the external momentum p but are rather dominated by the deuteron binding momentum (at least for diagram (c) this is straightforward to see). This means that compared to the simple one-nucleon-exchange diagram (without a photon) they are both suppressed by a factor $\alpha M_N/Q$. Consistent with this one finds by direct numerical evaluation that they are 7% (b) and 15% effects (c) at the zero-momentum scattering threshold.

We can summarize these findings by saying that unless a diagram directly exhibits the (regulated) Coulomb pole, it is not enhanced and thus a small electromagnetic correction to the same diagram topology without Coulomb-photon exchange. The enhanced Coulomb

⁶ For a related approach in the pionful theory, see also Ref. [44].

contributions are particularly large in the threshold region (where p is very small) and should thus be iterated to all orders. The calculations in Refs. [23, 26] neglect both diagrams (b) and (c) as well as all diagrams involving more than one Coulomb photon, giving them an *a priori* uncertainty of 7–15 percent. In Sec. VI E, we will critically assess this approach.

To conclude the topic for the moment we point out again that the power counting discussed here is specifically designed to account for Coulomb contributions that become strong in low-momentum scattering. At larger momenta, where the Coulomb parameter $\alpha M_N/p$ becomes small, it would suffice to not iterate any Coulomb diagrams but rather include them strictly perturbatively. However, exactly because they become small we assume that it also does not spoil the calculation to iterate them everywhere. As we will discuss in Sec. V B, for calculations in the bound-state regime the counting definitely has to be modified because there all loop-momentum scales are set by the binding momentum of the bound state. Based on the findings there, we will then argue in Section VI E that the same counting—which is actually simpler—should also be used in the scattering regime. For the moment, however, we proceed as in Ref. [26] and include only the Coulomb diagrams (a) and (d).

D. Three-nucleon forces

In Sec. VI we will present numerical evidence that without refitting the three-nucleon force $H(\Lambda)$ the doublet-channel proton–deuteron system is not properly renormalized beyond leading order. Indeed, it has been shown recently [28] based on analytical arguments that a new three-nucleon counterterm is needed to renormalize the charged sector at next-to-leading order in a fully-perturbative framework (*i.e.*, without partial resummation of effective-range corrections).

The expression in Eq. (6) is $SU(4)$ symmetric and can be rewritten as a structure of the form $(N^\dagger N)^3$. From this, it is simple to construct three-nucleon interactions which can be added in charged systems by using the charge operator $\hat{Q}_N = (\mathbf{1} + \tau_3)/2$. The case of two charged particles is relevant for the p – d system: $(N^\dagger \hat{Q}_N N)^2 (N^\dagger N)$. Using Fierz-transformations, one can show that its spin-isospin structure is different from $(N^\dagger N)^3$, and that it is up to a numerical constant identical to the form proposed in Ref. [28]. This interaction acts by construction only in the p – d system, and not in the n – d one, while $(N^\dagger N)^3$ acts in both systems, with the same strength. One can also write down interaction terms of the form

$$\mathcal{L}'_3 = \frac{M_N H_{n-d}(\Lambda)}{3\Lambda^2} \hat{O}_{Nd, Nt}^{n-d, 1/2} + \frac{M_N H_{p-d}(\Lambda)}{3\Lambda^2} \hat{O}_{Nd, Nt}^{p-d, 1/2}, \quad (23)$$

with operators $\hat{O}_{Nd, Nt}^{n-d, 1/2}$ and $\hat{O}_{Nd, Nt}^{p-d, 1/2}$ similar to the structure in Eq. (6), but projected in such a way that they only act in the n – d and p – d doublet channels, respectively.

III. INTEGRAL EQUATIONS

According to the power counting certain diagrams have to be resummed to all orders in order to calculate N – d scattering amplitudes in pionless EFT. The resulting integral equations are formally Lippmann–Schwinger equations (with non-trivial two-body propagators). In the following, we generically use the calligraphic letter \mathcal{T} to denote their solutions and indicate with appropriate subscripts which system we are referring to. In order to obtain

the quantum-mechanical T-matrix one has to include an overall minus sign and multiply with the deuteron wave function renormalization factor, *i.e.*,

$$T(E; \mathbf{k}, \mathbf{p}) = -Z_0 \mathcal{T}(E, \mathbf{k}, \mathbf{p}), \quad (24)$$

cf. Appendix A. Throughout this paper we write “ \mathcal{T} -matrix” (or simply “amplitude”) to indicate this distinction. We denote the incoming and outgoing center-of-mass momenta by \mathbf{k} and \mathbf{p} , respectively.

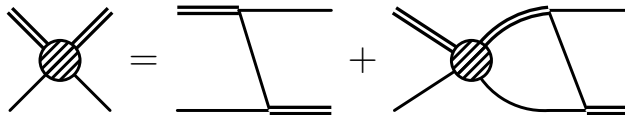


FIG. 4: Integral equation for the strong scattering amplitude \mathcal{T}_s in the quartet channel.

A. Neutron–deuteron quartet channel

Figure 4 shows a diagrammatic representation of the quartet-channel n - d amplitude, which is the simplest case one can have. The only interaction occurring here is the one-nucleon exchange diagram with deuteron legs on both sides. Including all spin-, isospin- and symmetry factors, it is given by

$$-\frac{iM_N y_d^2}{2} \cdot (\sigma^j \sigma^i)_\alpha^\beta \delta_a^b \cdot \frac{1}{\mathbf{k}^2 + \mathbf{k} \cdot \mathbf{p} + \mathbf{p}^2 - M_N E - i\varepsilon}. \quad (25)$$

Here, i and j are spin-1 indices and α, β (a, b) are spin-1/2 (isospin-1/2) indices. Since the spins of all three nucleons taking part in the reaction have to be aligned to produce a total spin-3/2 state, the Pauli principle prohibits here a three-nucleon contact interaction for which the particles have to occupy the same point in space. Furthermore, only the dibaryon field representing the deuteron can appear in the intermediate state.

Generically, we define the S-wave projected amplitude as

$$\mathcal{T}(E; k, p) = \frac{1}{2} \int_{-1}^1 d\cos\theta \mathcal{T}(E; \mathbf{k}, \mathbf{p}) \quad , \quad \theta = \theta_{\mathbf{k}\mathbf{p}} \quad , \quad k = |\mathbf{k}| \quad , \quad p = |\mathbf{p}|. \quad (26)$$

Applying this to the one-nucleon exchange shown in Eq. (25) yields the projected interaction kernel

$$K_s(E; k, p) \equiv \frac{1}{kp} Q_0 \left(\frac{k^2 + p^2 - M_N E - i\varepsilon}{kp} \right) \quad (27)$$

with the Legendre function of the second kind

$$Q_0(a) = \frac{1}{2} \int_{-1}^1 \frac{dx}{x+a} = \frac{1}{2} \log \left(\frac{a+1}{a-1} \right). \quad (28)$$

Here and in the following, the subscript “s” is used to denote the strong part of the interaction. The unprojected \mathcal{T} -matrix has the same spin-isospin indices as the kernel function shown in Eq. (25), $\mathcal{T} = (\mathcal{T}^{ij})_{\alpha\alpha}^{\beta b}$. The n - d quartet channel is chosen by inserting

$i = (1-i2)/\sqrt{2}$ and $j = (1+i2)/\sqrt{2}$ for the deuteron spin-1 indices, $\alpha = \beta = 1$ for the nucleon spins, and $a = b = 2$ to select the neutron in isospin space. As done in Refs. [12, 30] we have used here a short-hand notation for the spin-1 indices i and j that includes prefactors to be used in a linear combination. Written out explicitly, the strong quartet-channel amplitude is accordingly given by

$$\mathcal{T}_s^q = \frac{1}{2} \left(\mathcal{T}_s^{11} + i (\mathcal{T}_s^{12} - \mathcal{T}_s^{21}) + \mathcal{T}_s^{22} \right)_{12} \quad (29)$$

and fulfills the integral equation

$$\mathcal{T}_s^q = -M_N y_d^2 K_s + \mathcal{T}_s^q \otimes [M_N y_d^2 D_d K_s] . \quad (30)$$

As in Ref. [26] we have introduced here the short-hand notation

$$A \otimes B \equiv \frac{1}{2\pi^2} \int_0^\Lambda dq q^2 A(\dots, q) B(q, \dots) \quad (31)$$

and used the propagator function D_d as defined in Eq. (20). As indicated in Eq. (31), we regulate all loop integrations with an explicit momentum cutoff Λ .

B. Proton–deuteron quartet channel

Turning to the p - d system, we repeat that according to Sec. II C the dominant Coulomb contribution is the bubble diagram shown in Fig. 3a. Its energy and momentum dependence is given by

$$K_{\text{bubble}}(E; \mathbf{k}, \mathbf{p}) = \frac{\mathcal{I}_{\text{bubble}}(E; \mathbf{k}, \mathbf{p})}{(\mathbf{k} - \mathbf{p})^2 + \lambda^2} , \quad (32)$$

where

$$\mathcal{I}_{\text{bubble}}(E; \mathbf{k}, \mathbf{p}) = \frac{\arctan \left(\frac{2\mathbf{p}^2 - \mathbf{k}^2 - \mathbf{k} \cdot \mathbf{p}}{\sqrt{3\mathbf{k}^2 - 4M_N E - i\epsilon} \sqrt{(\mathbf{k} - \mathbf{p})^2}} \right) + \arctan \left(\frac{2\mathbf{k}^2 - \mathbf{p}^2 - \mathbf{k} \cdot \mathbf{p}}{\sqrt{3\mathbf{p}^2 - 4M_N E - i\epsilon} \sqrt{(\mathbf{k} - \mathbf{p})^2}} \right)}{\sqrt{(\mathbf{k} - \mathbf{p})^2}} \quad (33)$$

is the expression for the bubble loop integral. It can be simplified by noting that due to the denominator in Eq. (32) the whole expression is dominated by terms with $\mathbf{p}^2 \approx \mathbf{k}^2$. When the expression appears under the dq integral, we analogously get $\mathbf{p}^2 \approx \mathbf{k}^2$ and can furthermore assume that $\mathbf{q}^2 \approx \mathbf{k}^2$ because of the pole at this position in the deuteron propagator. Inserting then the total center-of-mass energy,

$$E = E(k) = \frac{3k^2}{4M_N} - \frac{\gamma_d^2}{M_N} , \quad k = |\mathbf{k}| , \quad (34)$$

we get

$$\frac{\mathcal{I}_{\text{bubble}}(E; \mathbf{k}, \mathbf{p})}{(\mathbf{k} - \mathbf{p})^2 + \lambda^2} \approx \frac{1}{2|\gamma_d|} \frac{1}{(\mathbf{k} - \mathbf{p})^2 + \lambda^2} \quad (35)$$

by using the expansion $\arctan(x) = x + \mathcal{O}(x^3)$ —with $x = \sqrt{(\mathbf{k} - \mathbf{p})^2}/(2|\gamma_d|)$ up to corrections that are further suppressed by powers of $\sqrt{k^2 - p^2}/|\gamma_d|$ —in Eq. (33). The same

simplification, which effectively amounts to keeping only loop contributions with $q \sim p$, has also been used in Ref. [23]. We point out, however, that Eq. (35) explicitly relies on the energy being given by Eq. (34) and is thus not valid in the bound-state regime, where $E < -E_d = -\gamma_d^2/M_N$. The integral equation, shown diagrammatically in Fig. 5, can then be written as

$$\mathcal{T}_{\text{full}}^q = -M_N y_d^2 \left(K_s - \frac{1}{2} K_c^{(d)} \right) + \mathcal{T}_{\text{full}}^q \otimes \left[M_N y_d^2 D_d \left(K_s - \frac{1}{2} K_c^{(d)} \right) \right] \quad (36)$$

with the kernel function $K_c^{(d)}$ that includes the bubble diagram and, at next-to-leading order and beyond, also diagram 3(d),

$$K_c^{(d,t)}(E; k, p) = -\alpha M_N \times \left[\underbrace{\int_{-1}^1 d \cos \theta \frac{\mathcal{I}_{\text{bubble}}(E; \mathbf{k}, \mathbf{p})}{(\mathbf{k} - \mathbf{p})^2 + \lambda^2}}_{\text{LO}} + \underbrace{\frac{\rho_{d,t}}{2kp} Q \left(-\frac{k^2 + p^2 + \lambda^2}{2kp} \right)}_{\text{NLO}} \right] \\ \approx \frac{\alpha M_N}{2kp} Q \left(-\frac{k^2 + p^2 + \lambda^2}{2kp} \right) \left(\frac{1}{|\gamma_d|} - \rho_{d,t} \right). \quad (37)$$

The variant $K_c^{(t)}$ only enters in the doublet channel.

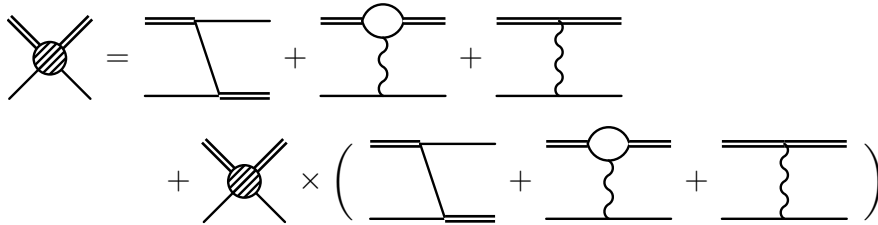


FIG. 5: Integral equation for the full (*i.e.* strong + Coulomb) scattering amplitude $\mathcal{T}_{\text{full}}$ in the quartet channel. The diagram with the photon coupled directly to the deuteron only enters at NLO and beyond.

C. Neutron–deuteron doublet channel

The equation for the doublet-channel amplitude is shown in Fig. 6. Since the spin-singlet dibaryon is now allowed to appear in the intermediate state, we have a coupled-channel system of two amplitudes that we call $\mathcal{T}_s^{\text{d},a}$ and $\mathcal{T}_s^{\text{d},b}$. Of these, the “upper part” $\mathcal{T}_s^{\text{d},a}$ corresponds directly to the n – d scattering process we are interested in, whereas $\mathcal{T}_s^{\text{d},b}$ only enters as an off-shell quantity because the spin-singlet dibaryon, being only a virtual bound state, cannot appear as a true asymptotic state.

Furthermore, with the spins coupled to a total spin $1/2$, the Pauli principle no longer prohibits a three-nucleon interaction, and indeed such a term is needed already at leading order to renormalize the system, as extensively discussed *e.g.* in the reviews [6, 8]. The corresponding diagrams have, however, for simplicity been omitted in Fig. 6. They can be reinstated by supplementing every one-nucleon exchange with a matching N – d contact

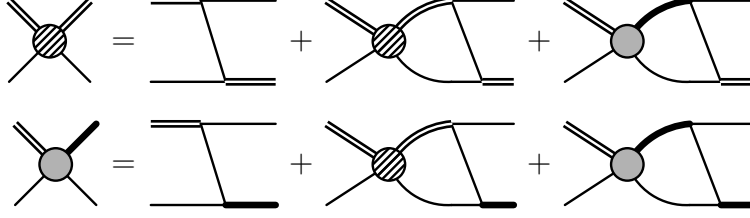


FIG. 6: Coupled-channel integral equation for the strong scattering amplitude \mathcal{T}_s in the doublet channel. The diagrams involving the three-body force have been omitted.

interaction from Eq. (6). With the doublet-channel projection,⁷

$$\mathcal{T}_s^{\text{d},a} = \frac{1}{3} (\sigma^i)_{\alpha}^{\alpha'} (\mathcal{T}_s^{\text{a},ij})_{\alpha'a}^{\beta'b} (\sigma^j)_{\beta'}^{\beta} \Big|_{\substack{a=b=2 \\ \alpha=\beta=1}}, \quad (38a)$$

$$\mathcal{T}_s^{\text{d},b} = \frac{1}{3} (\sigma^i)_{\alpha}^{\alpha'} (\mathcal{T}_s^{\text{b},iB})_{\alpha'a}^{\beta'b'} (\tau^B)_{b'}^b \Big|_{\substack{a=b=2 \\ \alpha=\beta=1}}, \quad (38b)$$

and introducing furthermore the abbreviations

$$g_{dd} = \frac{M_N y_d^2}{2}, \quad g_{dt} = \frac{M_N y_d y_t}{2}, \quad g_{tt} = \frac{M_N y_t^2}{2}, \quad (39)$$

the result can be written as

$$\begin{pmatrix} \mathcal{T}_s^{\text{d},a} \\ \mathcal{T}_s^{\text{d},b} \end{pmatrix} = \begin{pmatrix} g_{dd} \left(K_s + \frac{2H(\Lambda)}{\Lambda^2} \right) \\ -g_{dt} \left(3K_s + \frac{2H(\Lambda)}{\Lambda^2} \right) \end{pmatrix} + \begin{pmatrix} -g_{dd} D_d \left(K_s + \frac{2H(\Lambda)}{\Lambda^2} \right) & g_{dt} D_t \left(3K_s + \frac{2H(\Lambda)}{\Lambda^2} \right) \\ g_{dt} D_d \left(3K_s + \frac{2H(\Lambda)}{\Lambda^2} \right) & -g_{tt} D_t \left(K_s + \frac{2H(\Lambda)}{\Lambda^2} \right) \end{pmatrix} \otimes \begin{pmatrix} \mathcal{T}_s^{\text{d},a} \\ \mathcal{T}_s^{\text{d},b} \end{pmatrix}. \quad (40)$$

D. Proton–deuteron doublet channel: three-channel formalism

The p - d doublet-channel equation has a yet more complicated structure. Due to the fact that the electromagnetic interaction does not couple to isospin eigenstates we now need two different projections for the amplitude \mathcal{T}^b with the outgoing spin-singlet dibaryon:

$$\mathcal{T}_{\text{full}}^{\text{d},b1} = \frac{1}{3} (\sigma^i)_{\alpha}^{\alpha'} (\mathcal{T}_{\text{full}}^{\text{b},iB})_{\alpha'a}^{\beta'b'} (\mathbf{1} \cdot \delta^{B3})_{b'}^b \Big|_{\substack{a=b=1 \\ \alpha=\beta=1}}, \quad (41a)$$

$$\mathcal{T}_{\text{full}}^{\text{d},b2} = \frac{1}{3} (\sigma^i)_{\alpha}^{\alpha'} (\mathcal{T}_{\text{full}}^{\text{b},iB})_{\alpha'a}^{\beta'b'} (\mathbf{1} \cdot \delta^{B1} + i\mathbf{1} \cdot \delta^{B2})_{b'}^b \Big|_{\substack{a=1, b=2 \\ \alpha=\beta=1}}. \quad (41b)$$

The latter corresponds to the amplitude with the outgoing spin-singlet dibaryon in a pure p - p state. For the diagrams where this component appears in the intermediate state we have to insert the p - p propagator (17).

⁷ Setting $a = b = 2$ formally selects a neutron state. At this stage, however, in the absence of Coulomb effects and other isospin-breaking terms, one would find the same equations for $a = b = 1$.

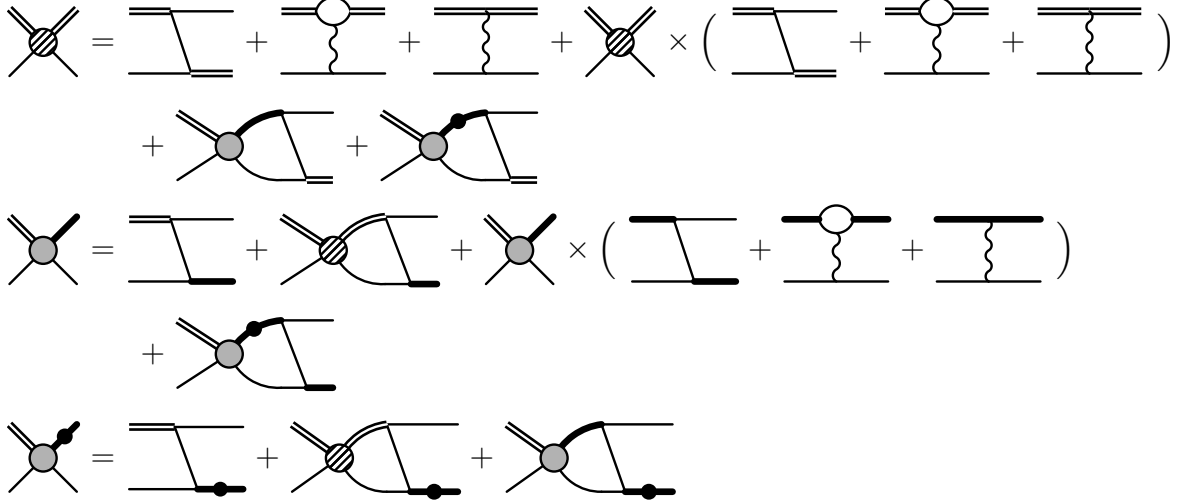


FIG. 7: Coupled-channel integral equation for the full (*i.e.*, strong + Coulomb) scattering amplitude $\mathcal{T}_{\text{full}}$ in the doublet channel. The diagrams representing the three-nucleon force have been omitted.

Diagrammatically, the resulting three-channel integral equation is shown in Fig. 7. It is given by

$$\begin{aligned}
\begin{pmatrix} \mathcal{T}_{\text{full}}^{\text{d,a}} \\ \mathcal{T}_{\text{full}}^{\text{d,b1}} \\ \mathcal{T}_{\text{full}}^{\text{d,b2}} \end{pmatrix} &= \begin{pmatrix} g_{dd} \left(K_s + \frac{2H(\Lambda)}{\Lambda^2} \right) \\ -g_{dt} \left(K_s + \frac{2H(\Lambda)}{3\Lambda^2} \right) \\ -g_{dt} \left(2K_s + \frac{4H(\Lambda)}{3\Lambda^2} \right) \end{pmatrix} + \begin{pmatrix} g_{dd} K_c^{(d)} \\ 0 \\ 0 \end{pmatrix} \\
&+ \begin{pmatrix} -g_{dd} D_d \left(K_s + \frac{2H(\Lambda)}{\Lambda^2} \right) & g_{dt} D_t \left(3K_s + \frac{2H(\Lambda)}{\Lambda^2} \right) & 0 \\ g_{dt} D_d \left(K_s + \frac{2H(\Lambda)}{3\Lambda^2} \right) & g_{tt} D_t \left(K_s - \frac{2H(\Lambda)}{3\Lambda^2} \right) & 0 \\ g_{dt} D_d \left(2K_s + \frac{4H(\Lambda)}{3\Lambda^2} \right) & -g_{tt} D_t \left(2K_s + \frac{4H(\Lambda)}{3\Lambda^2} \right) & 0 \end{pmatrix} \otimes \begin{pmatrix} \mathcal{T}_{\text{full}}^{\text{d,a}} \\ \mathcal{T}_{\text{full}}^{\text{d,b1}} \\ \mathcal{T}_{\text{full}}^{\text{d,b2}} \end{pmatrix} \\
&+ \begin{pmatrix} -g_{dd} D_d K_c^{(d)} & 0 & g_{dt} D_t^{pp} \left(3K_s + \frac{2H(\Lambda)}{\Lambda^2} \right) \\ 0 & -g_{tt} D_t K_c^{(t)} & -g_{tt} D_t^{pp} \left(K_s + \frac{2H(\Lambda)}{3\Lambda^2} \right) \\ 0 & 0 & -g_{tt} D_t^{pp} \times \frac{4H(\Lambda)}{3\Lambda^2} \end{pmatrix} \otimes \begin{pmatrix} \mathcal{T}_{\text{full}}^{\text{d,a}} \\ \mathcal{T}_{\text{full}}^{\text{d,b1}} \\ \mathcal{T}_{\text{full}}^{\text{d,b2}} \end{pmatrix} \quad (42)
\end{aligned}$$

with the Coulomb kernel functions $K_c^{(d,t)}$ as defined in Eq. (37). In writing Eq. (42) we have separated the terms in such a way that the Coulomb contributions can be easily identified.

Note that the terms involving $H(\Lambda)$ in Eq. (42) differ slightly from the version given in Ref. [26]. In particular, the contribution of $H(\Lambda)$ in the p - p channel was missing. However, this did not affect the final results since $H(\Lambda)$ was determined numerically from the triton binding energy.

The validity of the bubble-diagram approximation given in Eq. (35) is less clear in the doublet channel. For contributions with the spin-singlet dibaryon in the intermediate state, as they appear in Eq. (42), the argument based on the deuteron pole is actually not true.

However, for energies in the scattering regime, Eq. (35) is still a good approximation (numerically, a 15% effect at threshold and thus compatible with neglecting the diagram shown in Fig. 3c).

A more subtle point is that the above approximation also changes the ultraviolet scaling of the diagram, an effect for which it is difficult to judge *a priori* how important it is. Since the only true advantage of the approximation is that it—quite significantly—simplifies the calculation, but certainly does not improve it in any physical sense, it is probably best to not use it if possible. We will come back to this point in Sec. VI E.

E. Pure Coulomb scattering

In order to calculate Coulomb-subtracted phase shifts, we also need the amplitude for pure Coulomb scattering. Since the electromagnetic interaction in our approximation does not couple different channels, for both quartet-channel and doublet-channel p - d scattering it is given by the simple equation

$$\mathcal{T}_c = g_{dd} K_c^{(d)} - \mathcal{T}_c \otimes [g_{dd} D_d K_c^{(d)}] . \quad (43)$$

F. Higher-order corrections

From Eq. (37) one directly sees that the diagram with the photon coupled directly to a dibaryon (Fig. 3d and its analog with a spin-singlet dibaryon) is proportional to the effective range (ρ_d or ρ_t) and thus a correction that enters at next-to-leading order in the EFT power counting. This has already been mentioned in Sec. II C. Apart from that, the order of our calculation is determined by the expressions used for the dibaryon propagators.

The fully resummed propagators given in Eqs. (9) and (10) have spurious deep poles that do not correspond to actual physical bound states. In the quartet channel, the cutoff can be chosen low enough to avoid that pole. Due to the larger cutoff needed in the doublet channel, however, we cannot use the resummed propagators here. Instead, we follow the approach of Ref. [14] and use the perturbative expansions (more appropriately called “partially resummed propagators”) mentioned in Sec. II A. This still resums some higher-order effective-range contributions, but removes the unphysical pole.⁸

More precisely, at next-to-leading order we always use propagators $D_{d,t}^{\text{NLO}}$ that include a single insertion of the dibaryon kinetic energy operator and are thus linear in the effective range. At next-to-next-to-leading order (N²LO) the propagators $D_{d,t}^{\text{N}^2\text{LO}}$ for the doublet-channel calculation include corrections quadratic in the effective ranges, whereas in the quartet-channel we use the fully-resummed expression given by Eq. (9) together with a cutoff low enough to avoid the unphysical pole. This approach is chosen such that our quartet-channel results can be compared directly to those in Ref. [23].

Since the publication of Ref. [26] an agreement has been reached in the literature [14, 39, 45] that in the doublet channel, a second (energy-dependent) three-nucleon interaction is needed at N²LO for consistent renormalization. In Ref. [26] such a term has not been

⁸ This resummation procedure however affects the ultraviolet behavior of the propagators. The fully resummed expressions fall off faster than the leading-order propagators, whereas the perturbative expansions do not go to zero anymore for large p . This point will become important in Sec. VI.

included, meaning that the doublet-channel calculation presented there at N²LO is only a partial result. In fact, as we will discuss in Section VI E, with Coulomb effects included the question of correct renormalization in the double channel might have to be reconsidered already at next-to-leading order.

G. Numerical implementation

The integral equations presented in the previous sections have to be solved numerically. We do so by discretizing the integrals, using Gaussian quadrature, principal value integration to deal with the singularity of the deuteron propagator, and appropriate transformations of the integration domain. We use here the same method as described in Ref. [26]. The regulating photon mass λ is kept small in order to not modify the theory too much. By choosing an integration mesh-point distribution that puts emphasis on the Coulomb peak in the inhomogeneous parts of the integral equations and the low-momentum region, one obtains well-converged results and can even extrapolate (linearly) to the physical case $\lambda = 0$.

The experimental input parameters used in the calculation are the same as in Ref. [26] and summarized in Table I.

Parameter	Value	Ref.	Parameter	Value	Ref.
γ_d	45.701 MeV	[46]	ρ_d	1.765 fm	[7]
a_t	-23.714 fm	[47]	ρ_t	2.73 fm	[47]
a_C	-7.8063 fm	[48]	r_C	2.794 fm	[48]

TABLE I: Parameters used for the numerical calculation.

H. Scattering phase shifts

From the solutions of the integral equations we can obtain the S-wave scattering phase shifts as

$$\delta(k) = \frac{1}{2i} \log \left(1 + \frac{2ikM_N}{3\pi} Z_0 \mathcal{T}(E_k; k, k) \right). \quad (44)$$

As already mentioned, the \mathcal{T} -matrix is multiplied by the wave function renormalization constant Z_0 defined in Eq. (13). This procedure also removes the dependence of the amplitude on the coupling constant y_d , which so far we have kept in all equations.

For the p - d system, what has to be compared to experimental data are the Coulomb-subtracted phase shifts

$$\tilde{\delta}(k) \approx \delta_{\text{diff}}(k) \equiv \delta_{\text{full}}(k) - \delta_c(k), \quad (45)$$

where $\delta_{\text{full}}(k)$ is obtained from the full integral equation including both Coulomb and strong interactions and $\delta_c(k)$ is obtained from Eq. (43) which only includes the Coulomb interaction. This procedure (as opposed to calculating the pure Coulomb phase shift analytically in a purely two-body approximation) has the advantage of properly taking into account the finite cutoff, the EFT expansion, and the regulating photon mass λ .

Results for both quartet-channel and doublet-channel p - d phase shifts have been reported in Ref. [26]. Upon closer examination it turns out that these should actually be taken with a grain of salt. This has already been hinted at when we discussed the power counting in

Sec. II C and the bubble-diagram approximation (35). Indeed, a more careful analysis of the bound-state regime that will be discussed in the following sections also sheds some new light on the scattering calculation, a point that we will finally come back to in Sec. VI E.

IV. TRINUCLEON WAVE FUNCTIONS

The most straightforward observable in the three-nucleon bound-state regime is the ${}^3\text{H}$ – ${}^3\text{He}$ binding-energy shift. It can be calculated in first-order perturbation theory by treating the Coulomb interaction as a small correction. In order to do this we need the wave functions that describe the trinucleon (triton) bound state. As illustrated diagrammatically in Fig. 8, at the bound-state pole the \mathcal{T} -matrix factorizes as

$$\mathcal{T}(E; k, p) = -\frac{\mathcal{B}^\dagger(k)\mathcal{B}(p)}{E + E_B} + \text{terms regular at } E = -E_B, \quad (46)$$

where the $\mathcal{B}(p)$ are what we call *amputated* wave functions or vertex factors. For a derivation of this relation, including the sign, see Appendix A.

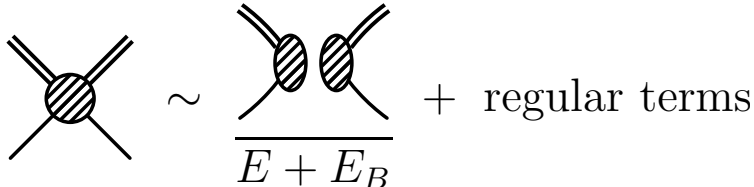


FIG. 8: Diagrammatic representation of the factorization of \mathcal{T} -matrix at the bound-state pole.

A. Homogeneous equation

For our coupled-channel problem, $\mathcal{T}(E; k, p)$ is a matrix in channel-space, and the wave functions will thus be vectors. We use here the three-channel equation structure even in the absence of Coulomb kernel functions in order to separate the component that in the p - d system (discussed below in Sec. V) corresponds to the spin-singlet dibaryon being in a pure p - p state. Our interaction kernel is then given by

$$\hat{K} \equiv \begin{pmatrix} -g_{dd} \left(K_s + \frac{2H(\Lambda)}{\Lambda^2} \right) & g_{dt} \left(3K_s + \frac{2H(\Lambda)}{\Lambda^2} \right) & g_{dt} \left(3K_s + \frac{2H(\Lambda)}{\Lambda^2} \right) \\ g_{dt} \left(K_s + \frac{2H(\Lambda)}{3\Lambda^2} \right) & g_{tt} \left(K_s - \frac{2H(\Lambda)}{3\Lambda^2} \right) & -g_{tt} \left(K_s + \frac{2H(\Lambda)}{3\Lambda^2} \right) \\ g_{dt} \left(2K_s + \frac{4H(\Lambda)}{3\Lambda^2} \right) & -g_{tt} \left(2K_s + \frac{4H(\Lambda)}{3\Lambda^2} \right) & -g_{tt} \times \frac{4H(\Lambda)}{3\Lambda^2} \end{pmatrix}, \quad (47)$$

which is found from Eq. (42) by factoring out all propagators and omitting the $K_c^{(d,t)}$ entries. Inserting the factorization at the pole (46) into the Lippmann-Schwinger equation⁹ and taking the limit $E \rightarrow -E_B$ gives a homogeneous equation of the form

$$\vec{\mathcal{B}}_s = (\hat{K}\hat{D}) \otimes \vec{\mathcal{B}}_s \quad (48)$$

⁹ Note that the kernel matrix in Eq. (47) is not symmetric. To rigorously apply the bound-state factorization, one should symmetrize it first by rescaling the second row with a factor 3 and the third row with

with

$$\vec{\mathcal{B}}_s \equiv (\mathcal{B}_s^{\text{d},\text{a}}, \mathcal{B}_s^{\text{d},\text{b1}}, \mathcal{B}_s^{\text{d},\text{b2}})^T, \quad \hat{D} = \text{diag}(D_d, D_t, D_t), \quad (49)$$

The inhomogeneous interaction terms have dropped out here since they are regular as $E = -E_B$, and we have canceled the overall \mathcal{B}^\dagger terms from the factorization.

B. Normalization condition

In order to calculate quantities based on the wave functions \mathcal{B}_s it is important to normalize these correctly. To this end one has to take into account that the ‘‘potential’’ derived from the EFT we are using here, *i.e.*, the one-nucleon exchange kernel as given in Eqs. (25) and (27), is effectively energy-dependent. The proper normalization condition is

$$\left(\hat{D}\vec{\mathcal{B}}_s\right)^T \otimes \frac{d}{dE} \left(\hat{I} - \hat{K}\right) \Big|_{E=-E_B^{\text{3H}}} \otimes \left(\hat{D}\vec{\mathcal{B}}_s\right) = 1, \quad (50)$$

where we have defined the matrix of inverse propagators $\hat{I} = \text{diag}(I_d, I_t, I_t)$ with

$$I_{d,t}(E, q, q') = \frac{2\pi^2}{q^2} \delta(q - q') D_{d,t}(E; q)^{-1}. \quad (51)$$

A detailed derivation of this can again be found in Appendix A. Note, however, that the insight that energy-dependent interactions imply a nontrivial normalization condition for bound-state wave functions has been known since quite some time (see, for example, the overview by Agrawala *et al.* [49] and references therein).

The normalization condition derived above can be verified numerically by considering the residue of the \mathcal{T} -matrix at the bound-state pole. Following Hagen *et al.* [50] we define

$$Z = \lim_{E \rightarrow -E_B} (E + E_B) \int_0^\Lambda \frac{dq q^2}{2\pi^2} \int_0^\Lambda \frac{dq' q'^2}{2\pi^2} D(E, q) \mathcal{T}(E; q, q') D(E, q') \quad (52)$$

and call this quantity the Z -factor of the trinucleon state, or simply *trimer Z-factor*. As we will discuss shortly, for our coupled-channel system we need to sum over all components of the \mathcal{T} -matrix. In Eq. (52) we have written $D(E, q)$ to denote a generic dibaryon propagator.

Inserting the factorization of the \mathcal{T} -matrix at the pole as given in Eq. (46), we find that

$$\begin{aligned} Z &= \int_0^\Lambda \frac{dq q^2}{2\pi^2} \int_0^\Lambda \frac{dq' q'^2}{2\pi^2} D(-E_B, q) \mathcal{B}^\dagger(q) \mathcal{B}(q') D(-E_B, q') \\ &= \left| \int_0^\Lambda \frac{dq q^2}{2\pi^2} D(-E_B, q) \mathcal{B}(q) \right|^2, \quad (53) \end{aligned}$$

where the last equality follows by noting that the propagators are real in the bound-state regime. Of course, it is crucial here that the wave functions $\mathcal{B}(q)$ are normalized correctly, so

a factor 3/2. In practice, however, one can simply solve the homogeneous equation with the kernel as in Eq. (47) and insert the appropriate symmetrization factors whenever one calculates matrix elements from the solutions.

numerically calculating Z from both Eqs. (52) and (53) and showing that the results agree provides the means to verify our normalization condition (50) with an explicit calculation.

We now carry out this procedure for the triton wave functions in the two-channel formalism. In order to implement Eq. (52) we also need the part of the amplitude that describes the (unphysical) scattering of a spin-singlet dibaryon and a nucleon. The complete \mathcal{T} -matrix for the system is then given by

$$\hat{\mathcal{T}}_s^d = \begin{pmatrix} \mathcal{T}_s^{d,a} & \mathcal{T}_s^{d,c} \\ \mathcal{T}_s^{d,b} & \mathcal{T}_s^{d,d} \end{pmatrix}, \quad (54)$$

where the first column is determined by Eq. (40) and the second column is a solution of the analogous equation

$$\begin{pmatrix} \mathcal{T}_s^{d,c} \\ \mathcal{T}_s^{d,d} \end{pmatrix} = \begin{pmatrix} -g_{dt} \left(3K_s + \frac{2H(\Lambda)}{\Lambda^2} \right) \\ g_{tt} \left(K_s + \frac{2H(\Lambda)}{\Lambda^2} \right) \end{pmatrix} + \begin{pmatrix} -g_{dd}D_d \left(K_s + \frac{2H(\Lambda)}{\Lambda^2} \right) & g_{dt}D_t \left(3K_s + \frac{2H(\Lambda)}{\Lambda^2} \right) \\ g_{dt}D_d \left(3K_s + \frac{2H(\Lambda)}{\Lambda^2} \right) & -g_{tt}D_t \left(K_s + \frac{2H(\Lambda)}{\Lambda^2} \right) \end{pmatrix} \otimes \begin{pmatrix} \mathcal{T}_s^{d,c} \\ \mathcal{T}_s^{d,d} \end{pmatrix}. \quad (55)$$

The expression for the trimer Z -factor in terms of the \mathcal{T} -matrix is then

$$Z_{\mathcal{T}} = \lim_{E \rightarrow -E_B} (E + E_B) \sum_{i,j=1}^2 \left[\hat{D}_{ii} \otimes (\hat{\mathcal{T}}_s^d)_{ij} \otimes \hat{D}_{jj} \right], \quad (56)$$

where we have switched back to the short-hand notation of Section III (with the modification that $\hat{D} = \text{diag}(D_d, D_t)$ is only a 2×2 matrix here) and inserted a subscript \mathcal{T} in order to distinguish it from the expression in terms of the wave functions, which we write as

$$Z_{\mathcal{B}} = \sum_{i=1}^2 \left| \hat{D}_{ii} \otimes (\vec{\mathcal{B}}_s)_i \right|^2. \quad (57)$$

Numerically calculating $Z_{\mathcal{B}}$ is straightforward since it is just a simple integral over the normalized wave functions. Implementing the procedure to calculate $Z_{\mathcal{T}}$, on the other hand, is more delicate since in order to numerically obtain the residue one has to rely on cancellations between large numbers. If, however, we approach the bound-state pole exponentially, *i.e.*, set

$$E(x) = -E_B + (E_B - E_0) \cdot \exp(-x), \quad (58)$$

where E_0 is some energy between the deuteron binding energy E_d and E_B , we find that indeed $Z_{\mathcal{T}}$ converges to $Z_{\mathcal{B}}$ as a function of the parameter x .¹⁰

We show this in Figs. 9 for a cutoff $\Lambda = 1000$ MeV. In the calculation we have used $E_0 = 1.1 \times E_d$, which means that at $x = 20$ the distance to the pole (which is always fixed to be exactly at $E_B = 8.4818$ MeV) is only about 10^{-8} MeV. Only if one goes even closer to

¹⁰ The authors would like to thank P. Hagen for suggesting this approach.

the pole ($x \gtrsim 25$), numerical difficulties become significant and $Z_{\mathcal{T}}$ starts to visibly deviate from $Z_{\mathcal{B}}$. At $x = 20$, $Z_{\mathcal{T}}$ still agrees with $Z_{\mathcal{B}}$ to within about 1.5%. At other cutoffs one finds the same overall behavior.¹¹ We take the above findings as a clear numerical verification underlining the correctness of our normalization condition (50).

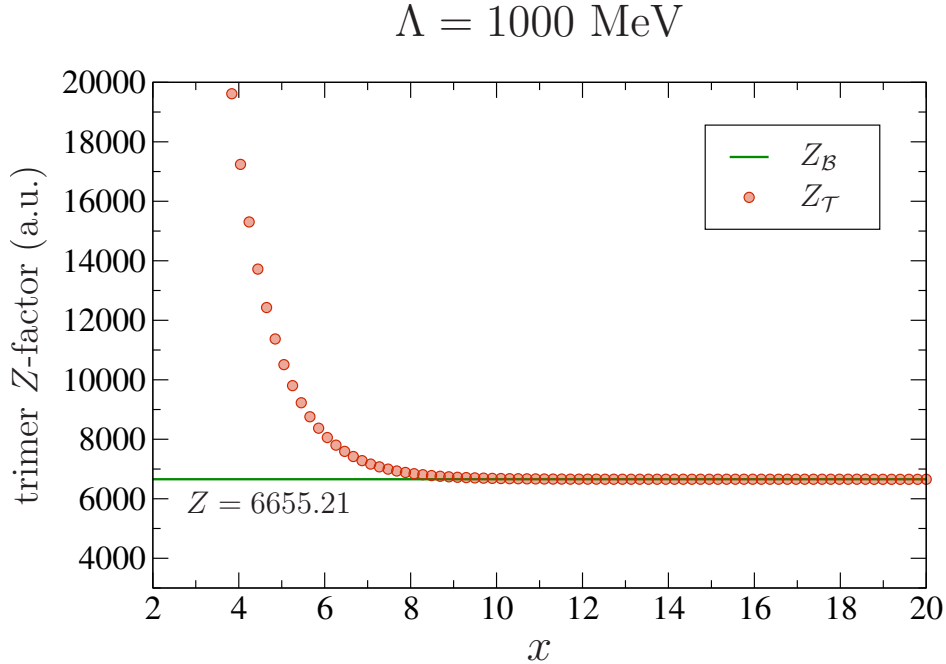


FIG. 9: Triton trimer Z factor (in arbitrary units, a.u.) for cutoff $\Lambda = 1000 \text{ MeV}$. x is the parameter in Eq. (58).

V. HELIUM-3 PROPERTIES

We are now finally in a position to discuss the Helium-3 system. In the first part of this section we will describe how to obtain the ${}^3\text{H}$ - ${}^3\text{He}$ binding energy shift in a perturbative approach based the normalized trinucleon wave functions \mathcal{B}_s . The results presented here correct and thus supersede those given in Ref. [26]. We will additionally describe how to obtain the ${}^3\text{He}$ binding energy nonperturbatively by locating the pole in the full \mathcal{T} -matrix. The results of both calculations will be shown and discussed in Subsec. V C.

¹¹ Note, however, that the numerical value of the Z -factor varies significantly with the cutoff. This can be understood by noting that the way we have defined it in Eqs. (52) and (53), Z is an *unrenormalized* quantity. For the current discussion where we are only interested in establishing the agreement of $Z_{\mathcal{T}}$ and $Z_{\mathcal{B}}$, however, this is of no importance.

A. Energy shift in perturbation theory

In Ref. [26] the ${}^3\text{H}$ - ${}^3\text{He}$ binding-energy difference was calculated using

$$\Delta E_C^{\text{old}} = \left(\hat{D}\vec{\mathcal{B}}_s\right)^T \otimes \text{diag}(V_C, V_C, 0) \otimes \left(\hat{D}\vec{\mathcal{B}}_s\right) \quad (59)$$

with the S-wave projected Coulomb potential

$$V_C(E; q, q') = -\frac{4\pi\alpha}{2qq'} Q_0 \left(-\frac{q^2 + q'^2 + \lambda^2}{2qq'} \right) \quad (60)$$

in momentum space. The prediction for the ${}^3\text{He}$ binding energy is then given by

$$-E_B^{{}^3\text{He}} = -E_B^{{}^3\text{H}} + \Delta E_C^{\text{old}}. \quad (61)$$

However, the naïve approach in Eq. (59) is actually not correct. By taking the simple matrix elements of the Coulomb potential between the wave functions $\vec{\mathcal{B}}_s$ in the nucleon-dibaryon formalism, one effectively couples the photon directly to the dibaryon. However, as discussed in Section II C, this coupling only enters at next-to-leading order in the EFT power counting.

More subtle, but no less important, is to realize that the expression in Eq. (59) is not renormalized correctly. By considering the terms that enter in the normalization condition (50) we find that formally the wave functions $\vec{\mathcal{B}}_s$ are proportional to the EFT coupling constants y_d and y_t . In the results for physical quantities this dependence has to drop out, just as it does in the scattering calculation where the deuteron wave function renormalization constant cancels the y_d -dependence of the \mathcal{T} -matrix.

In fact, Eq. (59) neglects the three-body nature of the problem. To correct this, what should be done is to calculate the diagram shown in Fig. 10a at leading order and only add the contribution shown Fig. 10b as an NLO-correction. Effectively, this amounts to calculating

$$\Delta E_C^{\text{new}} = \left(\hat{D}\vec{\mathcal{B}}_s\right)^T \otimes \hat{K}_C \otimes \left(\hat{D}\vec{\mathcal{B}}_s\right) \quad (62)$$

with the matrix

$$\hat{K}_C = \text{diag}(-g_{dd}K_c^{(d)}, -g_{tt}K_c^{(t)}, 0). \quad (63)$$

The kernel functions K_c here are the same that appear in the integral equation for the full scattering amplitude, with the leading-order contribution given by the bubble diagram, Fig. 3a, and the direct coupling to the dibaryon only entering at next-to-leading order. As we will discuss in more detail in the next section, it is important here to not use the approximation (35) for the bubble diagram but rather include the full expression given in the first line of Eq. (37).

The new procedure takes into account the EFT expansion and, since \hat{K}_C is proportional to $y_{d,t}^2$, ΔE_C^{new} is also renormalized correctly. However, the picture is still not complete. As shown in Fig. 11, there are also contributions to the energy shift that arise from Coulomb-photon diagrams not taken into account so far. For the scattering calculation it was argued that they can be neglected, but we already mentioned at the end of Section II C that the power counting has to be modified in the bound-state regime. As we will discuss shortly, these additional diagrams actually are important and should be taken into account in the energy-shift calculation. The complete \hat{K}_C then becomes a non-diagonal matrix.



FIG. 10: Diagrams contributing to the ${}^3\text{H}-{}^3\text{He}$ binding energy difference in perturbation theory. (a) Leading-order diagram. (b) NLO-correction.



FIG. 11: Additional diagrams contributing to the ${}^3\text{H}-{}^3\text{He}$ binding energy difference in perturbation theory. (a) Box diagram. (b) Triangle diagram.

B. Nonperturbative calculation

In Ref. [24], Ando and Birse calculate the ${}^3\text{He}$ binding energy in pionless EFT by using a nonperturbative framework that involves the full off-shell Coulomb T-matrix. As already discussed by Kok *et al.* in Refs. [51, 52], the latter complication is not actually necessary in the bound-state regime. In this section we carry out a calculation analogous to that of Ando and Birse, but only involving Coulomb photons. The resulting equation structure is still quite complex, but much simpler and in particular easier to handle numerically than that of Ref. [24].

1. Diagram scaling in the bound-state regime

At this point it is important to recall from Section II C that the Coulomb diagrams in Figs. 3b and 3c, which in the following we simply refer to as the *box* and *triangle* diagrams, respectively, are not small *per se*, but rather that the bubble diagram, Fig. 3a, is enhanced in the low-energy scattering regime due to the Coulomb singularity at zero momentum transfer. That effect is particularly prominent in the inhomogeneous part of the integral equation, where one directly hits the Coulomb pole in the on-shell limit, so that the expression is only rendered finite by the regulating photon mass λ .

In the bound-state regime this is no longer the case. There are no inhomogeneous terms that could exhibit a Coulomb peak, and since all loops are dominated by the binding momentum of the bound-state under consideration, the dibaryon propagators do not further enhance integration domains of small momentum transfer.

The consequence of all this is that if the Helium-3 binding energy is calculated directly from the p - d integral equation (in an approach that is nonperturbative compared to the one discussed in Sec. V A), then all $\mathcal{O}(\alpha)$ Coulomb diagrams should be treated on an equal

footing and be included in the calculation. Furthermore, for the integral in the bubble diagram we have to use the full expression as given by Eq. (33) since the argument allowing the approximation given in Eq. (35) is not valid in the bound-state regime.

2. Full equation structure

The resulting full equation structure is shown diagrammatically in Fig. 12 and given by the expression

$$\begin{aligned}
\begin{pmatrix} \mathcal{T}_{\text{full}'}^{\text{d,a}} \\ \mathcal{T}_{\text{full}'}^{\text{d,b1}} \\ \mathcal{T}_{\text{full}'}^{\text{d,b2}} \end{pmatrix} &= \begin{pmatrix} g_{dd} \left(K_s + \frac{2H(\Lambda)}{\Lambda^2} \right) \\ -g_{dt} \left(K_s + \frac{2H(\Lambda)}{3\Lambda^2} \right) \\ -g_{dt} \left(2K_s + \frac{4H(\Lambda)}{3\Lambda^2} \right) \end{pmatrix} + \begin{pmatrix} g_{dd} \left(K_c^{(d)} + K_{\text{box}} \right) \\ -g_{dt} K_{\text{box}} \\ -2g_{dt} K_{\text{tri}}^{(\text{in})} \end{pmatrix} \\
&+ \begin{pmatrix} -g_{dd} D_d \left(K_s + \frac{2H(\Lambda)}{\Lambda^2} \right) & g_{dt} D_t \left(3K_s + \frac{2H(\Lambda)}{\Lambda^2} \right) & 0 \\ g_{dt} D_d \left(K_s + \frac{2H(\Lambda)}{3\Lambda^2} \right) & g_{tt} D_t \left(K_s - \frac{2H(\Lambda)}{3\Lambda^2} \right) & 0 \\ g_{dt} D_d \left(2K_s + \frac{4H(\Lambda)}{3\Lambda^2} \right) & -g_{tt} D_t \left(2K_s + \frac{4H(\Lambda)}{3\Lambda^2} \right) & 0 \end{pmatrix} \otimes \begin{pmatrix} \mathcal{T}_{\text{full}'}^{\text{d,a}} \\ \mathcal{T}_{\text{full}'}^{\text{d,b1}} \\ \mathcal{T}_{\text{full}'}^{\text{d,b2}} \end{pmatrix} \\
&+ \begin{pmatrix} -g_{dd} D_d \left(K_c^{(d)} + K_{\text{box}} \right) & 3g_{dt} D_t K_{\text{box}} & g_{dt} D_t^{pp} \left(3K_s + 3K_{\text{tri}}^{(\text{out})} + \frac{2H(\Lambda)}{\Lambda^2} \right) \\ g_{dt} D_d K_{\text{box}} & -g_{tt} D_t \left(K_c^{(t)} - K_{\text{box}} \right) & -g_{tt} D_t^{pp} \left(K_s + K_{\text{tri}}^{(\text{out})} + \frac{2H(\Lambda)}{3\Lambda^2} \right) \\ 2g_{dt} D_d K_{\text{tri}}^{(\text{in})} & -2g_{dt} D_t K_{\text{tri}}^{(\text{in})} & -g_{tt} D_t^{pp} \times \frac{4H(\Lambda)}{3\Lambda^2} \end{pmatrix} \\
&\otimes \begin{pmatrix} \mathcal{T}_{\text{full}'}^{\text{d,a}} \\ \mathcal{T}_{\text{full}'}^{\text{d,b1}} \\ \mathcal{T}_{\text{full}'}^{\text{d,b2}} \end{pmatrix}, \quad (64)
\end{aligned}$$

which, albeit quite complex, is a direct extension of Eq. (42). We use primes in the subscript to indicate the inclusion of the additional Coulomb contributions compared to Eq. (42). The first of these, K_{box} , is initially given by a rather complicated expression but can be simplified to [53]

$$\begin{aligned}
K_{\text{box}}(E; k, p) &= -\alpha M_N \\
&\times \frac{1}{2} \int_{-1}^1 d\cos\theta \left\{ \frac{\arctan\left(\frac{2\mathbf{p}^2 - \mathbf{k}^2 - \mathbf{k}\cdot\mathbf{p}}{\sqrt{3\mathbf{k}^2 - 4M_N E - i\varepsilon}\sqrt{(\mathbf{k}-\mathbf{p})^2}}\right) + \arctan\left(\frac{2\mathbf{k}^2 - \mathbf{p}^2 - \mathbf{k}\cdot\mathbf{p}}{\sqrt{3\mathbf{p}^2 - 4M_N E - i\varepsilon}\sqrt{(\mathbf{k}-\mathbf{p})^2}}\right)}{(\mathbf{k}^2 + \mathbf{p}^2 + \mathbf{k}\cdot\mathbf{p} - M_N E - i\varepsilon)\sqrt{(\mathbf{k}-\mathbf{p})^2}} \right. \\
&\quad \left. - \frac{\lambda}{(\mathbf{k}^2 + \mathbf{p}^2 + \mathbf{k}\cdot\mathbf{p} - M_N E - i\varepsilon)^2} \right\}, \quad (65)
\end{aligned}$$

which is valid up to (negligible) corrections of order λ^2 . This expression is obtained by writing the expression obtained from the Feynman diagram shown in Fig. 3(b) in such a way that a Taylor expansion in the photon mass λ can be carried out before performing the integration over one remaining Feynman parameter. More precisely, the expansion parameter is proportional to $\lambda/(\mathbf{k}^2 + \mathbf{p}^2 + \mathbf{k}\cdot\mathbf{p} - M_N E - i\varepsilon)^{1/2}$. Recalling that this is at

least of the order of the deuteron binding momentum γ_d (in the scattering regime) or even dominated by the trinucleon binding energy (in the bound-state regime), it is clear that the approximation in Eq. (65) is very good. We have checked numerically that this is indeed the case.¹²

For the triangle-diagram contributions one furthermore finds

$$K_{\text{tri}}^{(\text{out})}(E; k, p) = -\alpha M_N \times \frac{1}{2} \int_{-1}^1 d\cos\theta \frac{\mathcal{I}_{\text{tri}}(E; \mathbf{k}, \mathbf{p})}{\mathbf{k}^2 + \mathbf{p}^2 + \mathbf{k} \cdot \mathbf{p} - M_N E - i\varepsilon}, \quad (66a)$$

$$K_{\text{tri}}^{(\text{in})}(E; k, p) = K_{\text{tri}}^{(\text{out})}(E; k, p), \quad (66b)$$

where the superscripts indicate whether the Coulomb-photon exchange is on the incoming (left) or outgoing (right) side of the diagram. The loop function appearing in Eq. (66a) is given by

$$\begin{aligned} \mathcal{I}_{\text{tri}}(E; \mathbf{k}, \mathbf{p}) = & \frac{i}{2\sqrt{\mathbf{k}^2/4 + \mathbf{k} \cdot \mathbf{p} + \mathbf{p}^2}} \\ & \times \left\{ \log \left(\frac{i(\mathbf{k}^2/2 - \mathbf{k} \cdot \mathbf{p} - \mathbf{p}^2 - \lambda^2 - M_N E - i\varepsilon)}{\sqrt{\mathbf{k}^2/4 + \mathbf{k} \cdot \mathbf{p} + \mathbf{p}^2}} + 2\sqrt{\lambda^2 + 3\mathbf{k}^2/4 - M_N E - i\varepsilon} \right) \right. \\ & \left. - \log \left(\frac{i(\mathbf{k}^2 + \mathbf{p}^2 + \mathbf{k} \cdot \mathbf{p} - \lambda^2 - M_N E - i\varepsilon)}{\sqrt{\mathbf{k}^2/4 + \mathbf{k} \cdot \mathbf{p} + \mathbf{p}^2}} + 2\lambda \right) \right\}. \quad (67) \end{aligned}$$

The spin and isospin projections for both diagrams are completely analogous to those for the simple one-nucleon exchange diagram, with additional projection operators from the photon vertices ensuring that contributions forbidden by charge conservation vanish as they should.

C. Leading-order results

1. Binding energies

The leading-order results for the ${}^3\text{He}$ binding energy (with the three-body force $H(\Lambda)$ fixed, for each cutoff Λ , such that the experimental triton binding energy is reproduced by the calculation in the n - d channel) are summarized in Fig. 13. The lower dashed curve shows the result of the naïve calculation reported in Ref. [26]. The upper dashed curve is the corrected result according to Eq. (62), where only the bubble diagram is taken into account at leading order. The effect of including all $\mathcal{O}(\alpha)$ Coulomb diagrams (that are leading order in the EFT counting) is shown by the lower solid curve, whereas the upper solid curve shows the result obtained from the nonperturbative calculation described in Section V B. For comparison, the experimental ${}^3\text{He}$ and ${}^3\text{H}$ binding energies are indicated as dotted lines and the cutoff dependence of the three-nucleon force $H(\Lambda)$ is shown as a thin dashed curve.

¹² An expression for the box diagram without expansion in λ can be obtained from the expression given in Eq. (90) in Sec. VII A 2 by replacing the T-matrix $T_{C,\lambda}$ discussed in that section with a simple Coulomb-photon propagator.

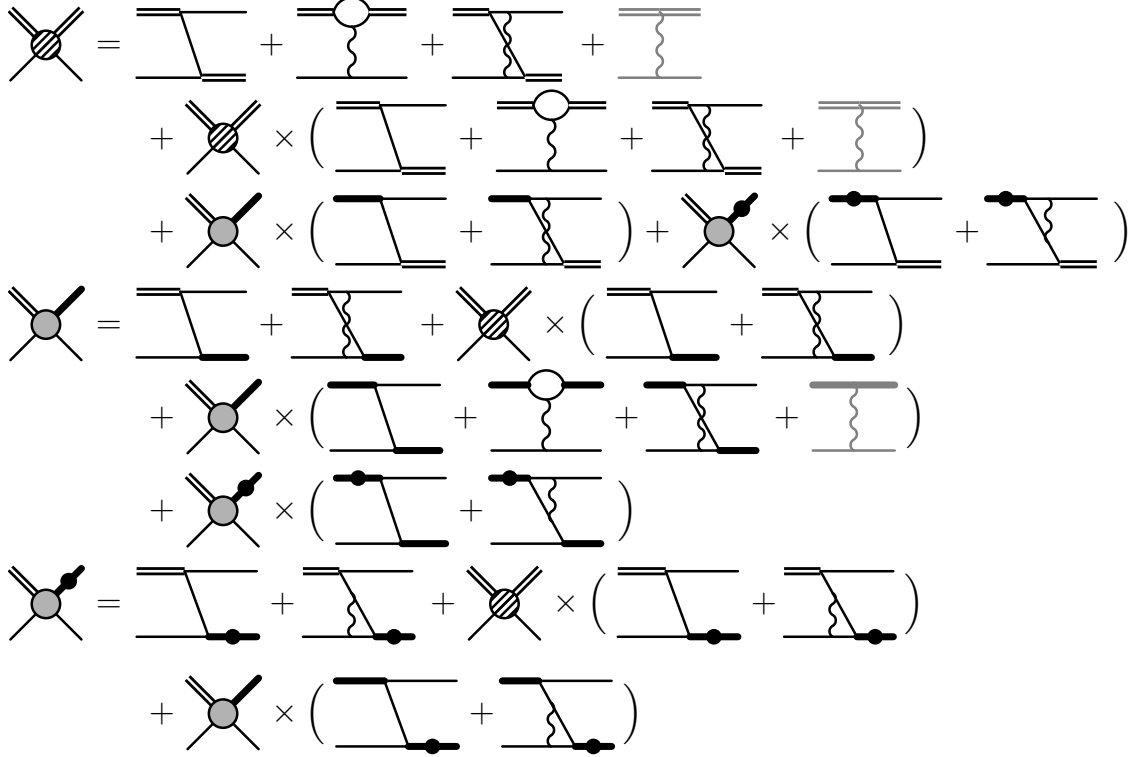


FIG. 12: Coupled-channel integral equation for the full scattering amplitude $\mathcal{T}_{\text{full}}$ used for the nonperturbative ${}^3\text{He}$ calculation. The diagrams representing the three-nucleon force have been omitted. The shaded diagrams with the photons coupled directly to the dibaryon only enter at NLO and beyond.

The most striking feature is that the new results, both from the perturbative and the nonperturbative calculation, do not show the fall-off at large cutoffs that was reported in Ref. [26] and is shown here by the lower dashed curve. An explanation for why this effect occurs in the naïve calculation will be given below in Section VI.

In fact, both new results are essentially stable beyond cutoffs of about 500 MeV. From Fig. 13 we furthermore see clearly that it is important to take into account all $\mathcal{O}(\alpha)$ Coulomb diagrams in the perturbative calculation. Comparing it with the result from the bubble diagram alone shows that the box and triangle diagrams together give more than half of the total energy shift (with the larger part coming from the triangle contributions). The nonperturbative result comes out closer to the experimental value than the perturbative one, as should be expected from that more complete calculation. Within the typical 30% uncertainty of a leading-order calculation in pionless EFT, however, they agree both with one another and with the experimental Helium-3 binding energy of about 7.72 MeV.¹³

Finally, the result obtained by Ando and Birse in Ref. [24] by using the full off-shell Coulomb T-matrix lies almost exactly on our curve. The small energy difference of about 0.004 MeV that we obtain at their cutoff $\Lambda = 380.689$ MeV is well beyond the accuracy

¹³ For the perturbative calculation this statement of course refers to the result where all $\mathcal{O}(\alpha)$ diagrams are included. The error estimate should in this case be taken as 30% of the *energy shift* (since that is what is calculated), which then gives a marginal agreement with the experimental value.

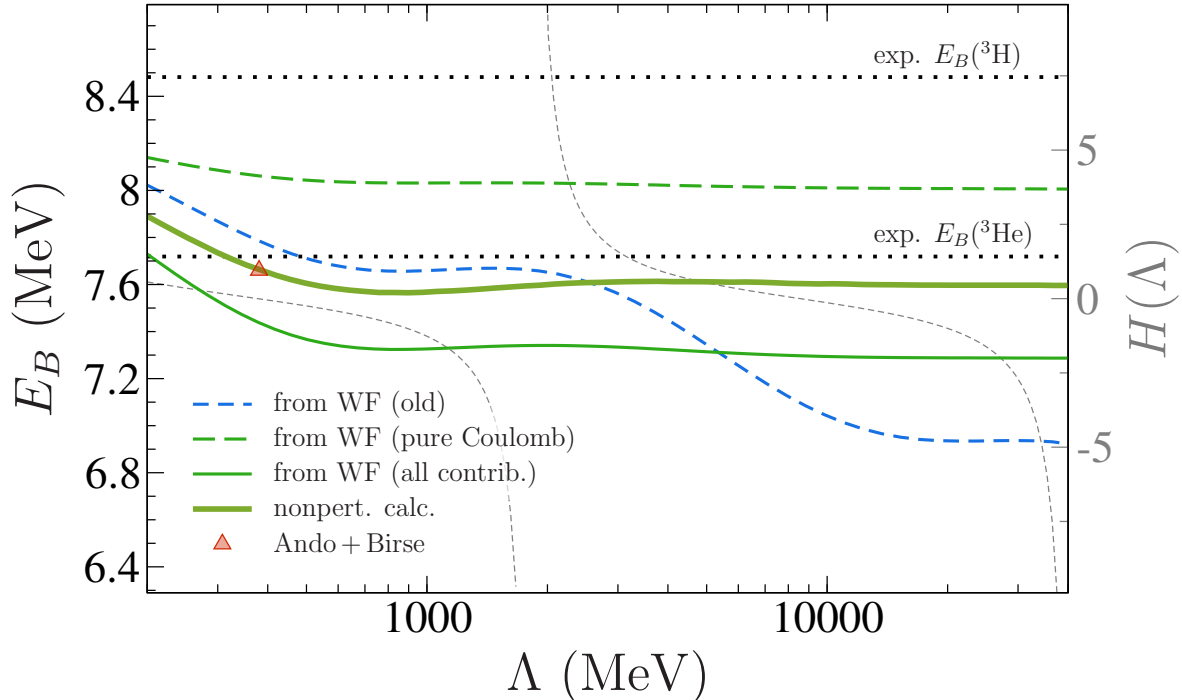


FIG. 13: Leading-order predictions for the ${}^3\text{He}$ binding energy as a function of the cutoff. Lower dashed curve: result from the naïve calculation reported in Ref. [26]. Upper dashed curve: corrected result according to Eq. (62). Lower solid curve: corrected result including all $\mathcal{O}(\alpha)$ Coulomb diagrams. Upper solid curve: nonperturbative result according to Section VB. Red triangle: result from Ref. [24]. Dotted lines: experimental values for the ${}^3\text{H}$ and ${}^3\text{He}$ binding energies. Thin dashed curve: cutoff-dependence of three-nucleon force.

of the calculation and cannot be resolved in the plot.¹⁴ This is in perfect agreement with the conclusion of Kok *et al.* [51, 52] that a Coulomb-photon approximation should be well justified in the bound-state regime.

2. Wave functions

From the new equation structure (64) we can also obtain Helium-3 wave functions. In Fig. 14 we show a representative plot, calculated at a cutoff $\Lambda = 400$ MeV. The three components of the wavefunction are labelled by the outgoing dibaryon field (“leg”) in the corresponding channel. The solid curves indicate the result obtained from the full equation including all leading Coulomb diagrams, whereas the dashed curves are obtained by calculating simple trinucleon wave functions (without Coulomb effects) for a system in which the three-nucleon force was fixed to reproduce the experimental ${}^3\text{He}$ binding energy. Both are normalized according to the condition (50) with the interaction \hat{K} set to the appropriate form.

¹⁴ Ando and Birse use the single cutoff $\Lambda = 380.689$ MeV for their calculation because they find that the three-nucleon vanishes there. We find this zero of $H(\Lambda)$ at $\Lambda \approx 377.69$ MeV instead. This small discrepancy is most likely due to differences in the numerical implementation and negligible here.

Comparing the two results, one finds that low-momentum modes are suppressed in the wave functions from the full calculation compared to the simple trinucleon result. This is in good agreement with what one naïvely expects from the repulsive Coulomb force: it is particularly strong for small relative momenta of the charged subsystems, thus lowering the probability of the system to be in such a state. For the wave function component where the dibaryon is in a pure p - p state, this does not apply because in that case there is no Coulomb repulsion between the dibaryon and the third nucleon. Indeed, exactly this can also be seen in Fig. 14.

The wave functions obtained in this manner can be used as nonperturbative input quantities for other calculations, *e.g.*, for a consistent determination of the Helium-3 photodisintegration in pionless EFT, which is currently work in progress.

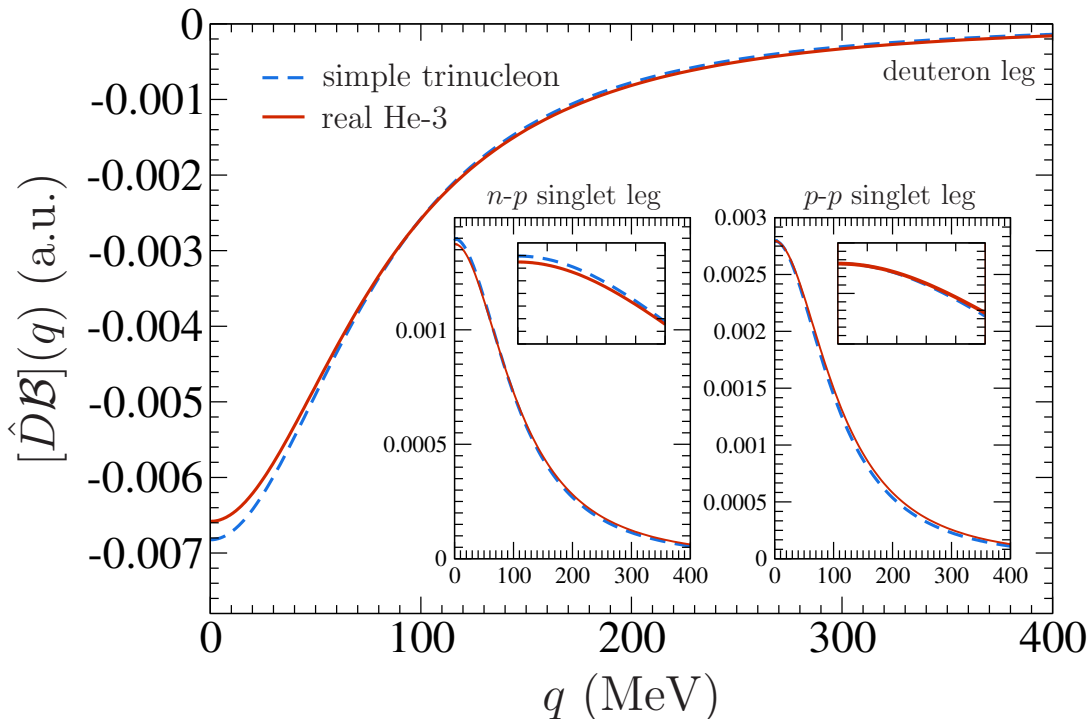


FIG. 14: Three-component Helium-3 wave functions (in arbitrary units, a.u.) calculated for a cutoff $\Lambda = 400$ MeV. The individual components are labelled by the outgoing dibaryon field (“leg”) in the corresponding channel. Solid curves: result from full calculation involving all leading Coulomb diagrams. Dashed curves: result from simple trinucleon calculation with the three-nucleon force fixed to give the experimental Helium-3 binding energy.

VI. THE COULOMB PROBLEM AT NEXT-TO-LEADING ORDER

From the promising results at leading order one might expect that going to next-to-leading order gives both more precision and better agreement with the experimental Helium-3 energy. However, as shown in Fig. 15, exactly the opposite is the case. The results from both the perturbative and the nonperturbative calculation are now closer to—or even above—the triton binding energy, which certainly does not make sense physically. Moreover, the results are strongly cutoff-dependent again and rise to even larger binding energies as the cutoff is

increased. From these findings one is led to suspect that our next-to-leading order calculation is not renormalized properly and that a new counterterm might be needed to renormalize the system at this order when Coulomb effects are included [27]. Recently, it was shown analytically that such a counterterm is indeed necessary [28]. That calculation was carried out in a framework where effective-range corrections are included fully perturbatively and uses an analytical investigation of the ultraviolet behavior of the kernels that enter in the integral equations. In the following we analyze the situation within the partial-resummation approach. As we will discuss below, the ultraviolet behavior of the dibaryon propagators—and thus the behavior of the three-body amplitudes—changes from order to order, which complicates the situation. Our analysis is therefore based largely on numerical investigations.

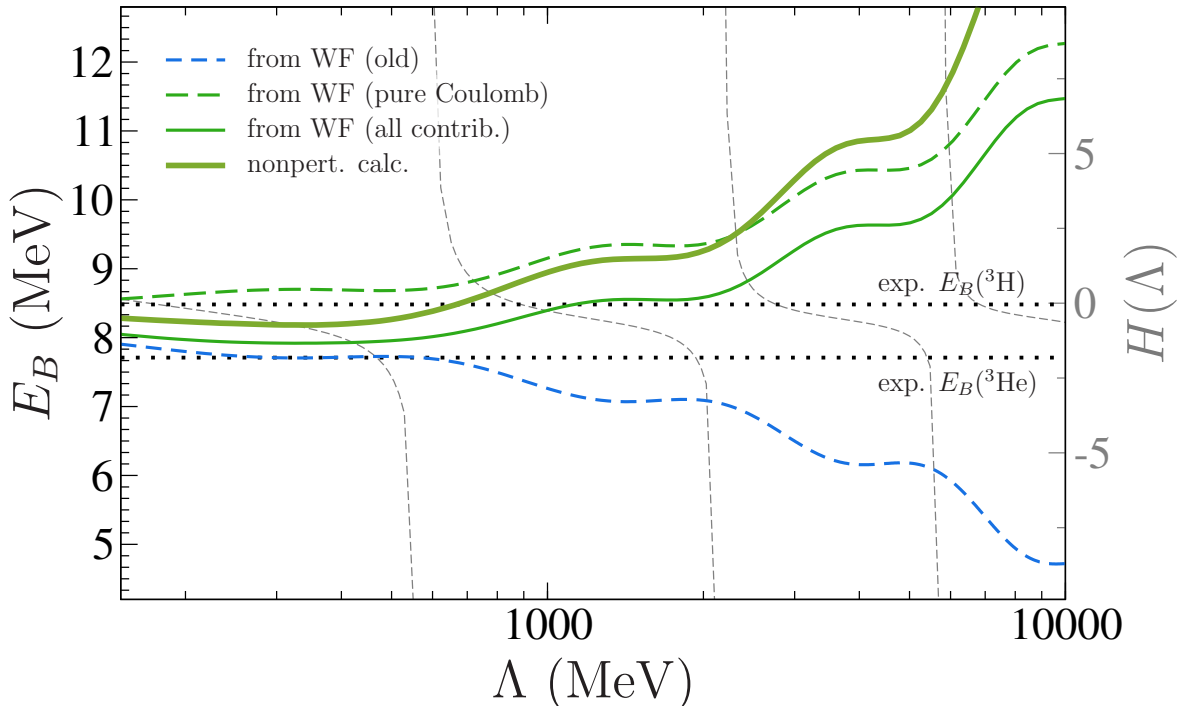


FIG. 15: NLO results for the ${}^3\text{He}$ binding energy as a function of the cutoff. The curves are as in Fig. 13.

A. Scaling of the dibaryon propagators

The ultraviolet scaling of the dibaryon propagators can directly be inferred from looking at their expressions. We consider here the deuteron propagator D_d as a representative example. At leading order, its scaling is

$$D_d^{\text{LO}}(E; q) \propto \frac{1}{-\gamma_d + \sqrt{\frac{3}{4}q^2 - M_N E - i\epsilon}} \sim \frac{1}{q} \text{ as } q \rightarrow \infty. \quad (68)$$

Upon going to next-to-leading order, this is multiplied by a factor proportional to the effective range,

$$D_d^{\text{NLO}}(E; q) = D_d^{\text{LO}}(E; q) \left[1 + \frac{\rho_d}{2} \cdot \frac{3q^2/4 - M_N E - \gamma_d^2}{-\gamma_d + \sqrt{\frac{3}{4}q^2 - M_N E - i\varepsilon}} \right], \quad (69)$$

such that the asymptotic behavior is changed to

$$D_d^{\text{NLO}}(E; q) \sim \text{const. as } q \rightarrow \infty. \quad (70)$$

Repeating this procedure in order to get the N²LO and higher-order propagators one even gets functions that are divergent ($\sim q$, $\sim q^2$, etc.) in the ultraviolet.

B. Ultraviolet behavior of the amplitude

In order to find the behavior of the wave functions $\mathcal{B}(p)$ introduced in Section IV, we first go back to the corresponding \mathcal{T} -matrix. As discussed, for example, in Ref. [14], for fixed E and k the n - d doublet channel amplitude $\mathcal{T}_s^{\text{d}}(E; k, p)$ has an asymptotic behavior determined by linear combinations of $p^{\pm i s_0 - 1}$ in the limit $p \rightarrow \infty$. It is the imaginary parts with $s_0 \approx 1.0064$ that give rise to the log-periodic behavior of the three-nucleon force $H(\Lambda)$ necessary to renormalize the system. What is important for the discussion here is the modulus of the scaling:

$$|\mathcal{T}_s^{\text{d}}(E; k, p)| \sim \frac{1}{p} \text{ as } p \rightarrow \infty. \quad (71)$$

Since the derivation of this is independent of the energy E , the same scaling also applies in the bound-state regime. In particular, it is inherited by the wave functions, such that also

$$|\mathcal{B}_s(p)| \sim \frac{1}{p} \text{ as } p \rightarrow \infty. \quad (72)$$

Indeed, as shown in Fig. 16, one also finds numerically that a plot of $p \cdot \mathcal{B}_s(p)$ against p shows a log-periodic behavior for large p with constant amplitude.

The analysis above is true at leading order. Numerically, we find at next-to-leading order the approximate scaling

$$|\mathcal{B}_s(p)| \sim |\mathcal{T}_s^{\text{d}}(E; k, p)| \sim \frac{1}{p^{3/2}} \text{ as } p \rightarrow \infty \quad (\text{NLO}) \quad (73)$$

for the wave functions (and the corresponding \mathcal{T} -matrix). This behavior is illustrated in Fig. 17, where we show the NLO wave functions up to large p , rescaled with a factor $p^{3/2}$. As in the leading-order case, this gives an oscillating function with approximately constant amplitude. Note that the oscillations are more rapid than at leading order and that the exact log-periodicity is broken at NLO. This is consistent with the behavior of the three-nucleon force $H(\Lambda)$ at next-to-leading order (*cf.* Fig. 15). The $p^{-3/2}$ fall-off can be seen more clearly in the inlay of Fig. 17, where the deuteron-leg component of the wave function (without rescaling) is plotted in a double-logarithmic scale. The same scaling behavior as reported here was found—and explained based on analytical considerations—for the scattering amplitude in Ref. [54].

To some extent this faster fall-off at next-to-leading order compensates the scaling of the dibaryon propagators, but, as we shall discuss below, not by enough to render the result convergent.

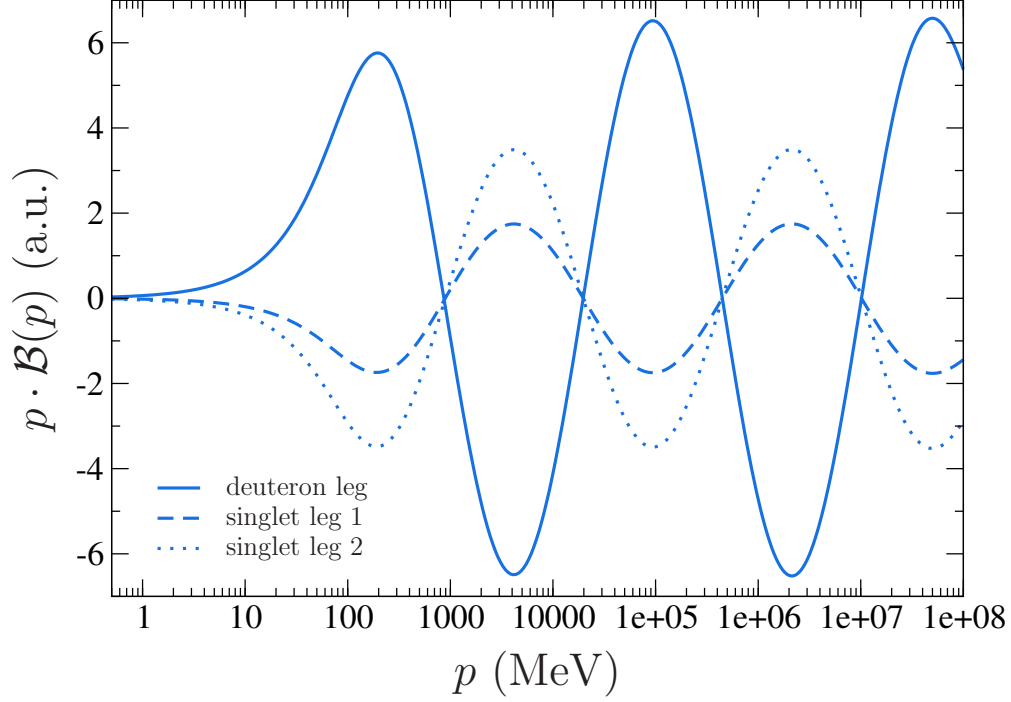


FIG. 16: Rescaled leading order trinucleon wave function $p \cdot \mathcal{B}_s(p)$ (in arbitrary units) as a function of the momentum p .

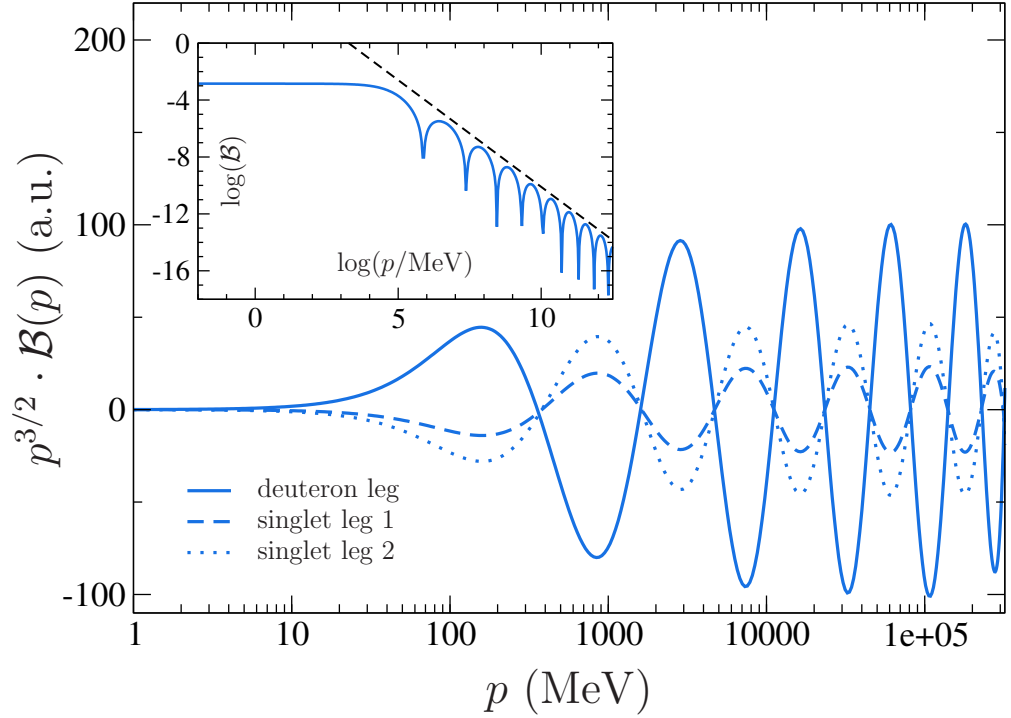


FIG. 17: Rescaled NLO trinucleon wave function $p^{3/2} \cdot \mathcal{B}_s(p)$ (in arbitrary units) as a function of the momentum p . The inlay shows the deuteron-leg component (without rescaling) in a double-logarithmic plot; the dashed line included there has a slope of exactly $-3/2$. For the other two components not included in the double-logarithmic plot, one finds exactly the same behavior.

C. Consequences

We first consider the situation in the leading-order case. The scaling of the Coulomb kernel in Eq. (62) is determined there by the large-momentum behavior of the bubble diagram without the approximation (35). From Eqs. (37) and (33) we then have

$$K_c^{\text{LO}}(E; k, q) \sim \frac{1}{q^3} \text{ as } q \rightarrow \infty. \quad (74)$$

Denoting in the following all loop momenta generically by q , we find

$$\left(\text{Fig. 10(a)}\right)_{\text{at LO}} \sim \left(\frac{1}{q}\right)_{\mathcal{B}}^2 \times \left(q^3\right)_{\text{loops}}^2 \times \left(\frac{1}{q}\right)_D \times \left(\frac{1}{q^3}\right)_{\text{kernel}} \sim \frac{1}{q} \quad (\text{LO}) \quad (75)$$

for the total scaling of the matrix element. Since this is the only contribution at leading order, the result for the energy shift converges as the cutoff is increased. From the same kind of analysis we can understand what led to the cutoff dependence in the result of Ref. [26]: the kernel V_C as defined in Eq. (60) only falls off like $1/q^2$ asymptotically such that the corresponding matrix element is logarithmically divergent.¹⁵

Considering finally the situation at next-to-leading order, we find that we can no longer avoid a divergent result. For the contribution of the bubble diagram we now obtain

$$\left(\text{Fig. 10(a)}\right)_{\text{at NLO}} \sim \left(\frac{1}{q^{3/2}}\right)_{\mathcal{B}}^2 \times \left(q^3\right)_{\text{loops}}^2 \times \left(q^0\right)_D^2 \times \left(\frac{1}{q^3}\right)_{\text{kernel}} \sim q^0 \quad (\text{NLO}), \quad (76)$$

which gives a logarithmic divergence. Even more problematic is the additional contribution entering at this order. For the kernel with the photon coupled directly to the dibaryon we have the scaling

$$\left(\text{Fig. 10(b)}\right) \sim \left(\frac{1}{q^{3/2}}\right)_{\mathcal{B}}^2 \times \left(q^3\right)_{\text{loops}}^2 \times \left(q^0\right)_D^2 \times \left(\frac{1}{q^2}\right)_{\text{kernel}} \sim q, \quad (77)$$

and thus a linear divergence. This again also applies to the old calculation involving V_C , which has the same scaling and thus diverges linearly as well. Indeed, by comparing the dashed curves in Figs. 13 and 15 we see that the NLO result has a much stronger cutoff dependence than at leading order, and can understand this now from the analysis carried out above.

Furthermore, we can explain as well why the new perturbative result at NLO looks almost like a mirror image of the old one. If we rewrite V_C in Eq. (60) by factoring out a $y_{d,t}^2$, the result is just the next-to-leading order contribution to $K_c^{(d,t)}$, but with the sign reversed. Due to the faster divergence of this term we barely see the effect of the “leading” bubble diagram at all.

¹⁵ The same kind of divergence occurs if the bubble diagram is approximated as in Eq. (35). However, as already mentioned repeatedly, the approximation is not valid in the bound-state regime, and the divergence that would appear if we were to use it there is just another manifestation of this fact.

D. Nonperturbative calculation

The result found from the nonperturbative calculation also exhibits a strong cutoff dependence at next-to-leading order, with the corresponding curve in Fig. 15 even rising somewhat faster than the perturbative result. From the analysis above one is led to suspect that again the scaling of the involved diagrams is the origin of this effect. In order to show this, we look at what kind of diagrams are generated when the bound-state integral equation is iterated.



FIG. 18: Two diagrams generated by iterating the bound-state integral equation.

Figure 18(a) shows a two-loop diagram with a Coulomb-photon exchange that is generated by iterating the equation once. Since the one-nucleon exchange also scales like $1/q^2$, we find a total scaling $\sim q^{1/2}$ for the diagram by applying the same kind of analysis as in the sections above. This indeed indicates a divergence.

We note that a similar diagram with two subsequent nucleon exchanges, shown in Fig. 18(b) actually has the same behavior for large momenta. This means that, based on the arguments above, one has a divergence already in the system without Coulomb effects. However, each nucleon exchange is always accompanied by a vertex from the three-nucleon force. According to the renormalization prescription this, three-nucleon force is adjusted at each cutoff in order reproduce a three-body experimental input (the triton binding energy, in our case). At NLO, this procedure effectively also absorbs the divergence into $H(\Lambda)$. The important point is now that by adding the Coulomb contributions into the equation after $H(\Lambda)$ is already fixed, the divergence problem is reintroduced.

At leading order, the situation is different because there the $1/q$ -scaling of the dibaryon propagators ensures that additional loops generated by iterating the integral equation do not create divergences, neither due to Coulomb photons nor due to the nucleon-exchange interaction. The three-nucleon force is needed in this case only to fix the oscillating behavior of the scattering amplitude [11].

E. Back to the scattering regime

The above findings also raise some questions concerning the NLO scattering calculation in the doublet channel. If the assertion that the system is not renormalized correctly is true, the effect should also show up in the cutoff-variation of the scattering phase shifts. Indeed, this is what we find. If we perform the phase-shift calculation with cutoffs of the same size as in Fig. 15 (up to $\Lambda \approx 10\,000$ MeV), the result does not seem to converge. Instead, the curves shown for four different cutoffs in the upper panel of Fig. 19 move upwards with increasing Λ .

One can of course take the stance, as we have done in Ref. [26] by varying the cutoff only between 200 and 600 MeV, that the cutoff in an EFT calculation should be taken of a natural

order of magnitude (defined by the scale of physics left out from the theory). According to Fig. 13, the leading-order Helium-3 results are indeed converged at these cutoffs. At next-to-leading order, however, Fig. 15 shows that the results are problematic already in that regime. With this in mind, considering cutoffs far beyond the natural size here and in the preceding sections is primarily a tool to expose and analyze this behavior more clearly.

Using the full equation structure (64) to fit the three-nucleon force such that it reproduces the experimental ${}^3\text{He}$ energy turns out to remove the strong cutoff dependence of the p - d results (without affecting the results for lower cutoffs very much), just as it does in the n - d system when $H(\Lambda)$ is fixed to reproduce the triton binding energy. This is shown in the lower panel of Fig. 19, where we plot the curves analogous to those in the upper panel obtained by re-fitting the three-nucleon force. For consistency we have used the same equation structure as in the bound-state regime—including the box and triangle diagrams and without the approximation of the bubble diagram—in the calculations of all phase-shift results shown in Fig. 19.

These findings are a further indication that in the p - d system there is a new three-body counterterm, which at least numerically can be absorbed by refitting $H(\Lambda)$. Such a situation could be accounted for by adding to the three-body Lagrangian (6) a piece proportional to the charge operator (making it vanish in the triton system). Since it is not forbidden by symmetry, such a term should be there, and the only question is at which order in the EFT counting it enters. As already mentioned, it has analytically been shown to enter at NLO in a fully perturbative calculation [28].

F. Neglected diagrams and the bubble approximation

Although the main motivation for deriving the full equation structure (64) with the box and triangle diagrams included was the nonperturbative Helium-3 calculation, with the complete expression at hand we are now also in a position to directly check the approximations made in the scattering regime. Based on the power counting described in Section II C, we neglected there the contributions from the box and triangle diagrams, and furthermore used the approximation given in Eq. (35) for the bubble diagram.

To avoid interference with the problematic situation at NLO discussed in the previous section, we go back to the leading-order calculation and show in Fig. 20 the old band (as given in Fig. 11 of Ref. [26]) together with the result obtained without approximating the bubble diagram (dashed curve) and furthermore what we get from the full equation with the box and triangle contributions included (solid curve). As before, all error bands were generated by varying the cutoff between 200 and 600 MeV, which is certainly sufficient at leading order.

The band from the full calculation overlaps well with the old result. In fact, if one takes the typical 30% of a leading-order pionless EFT calculation as a more appropriate estimate of the uncertainty, the two bands are almost indistinguishable. It would be tempting to interpret this as an *a posteriori* confirmation of both the Coulomb power counting for the scattering regime and the approximation used for the bubble diagram, if it were not for the result with only the bubble approximation turned off. Since the corresponding band in Fig. 20 is broader and consistently shifted upwards (for momenta k below about 70 MeV), it turns out that really the combination of both things—approximating the bubble diagram and neglecting the additional contributions—is important to get the same result as from the full calculation. This indicates that in the latter case there are some substantial cancellations

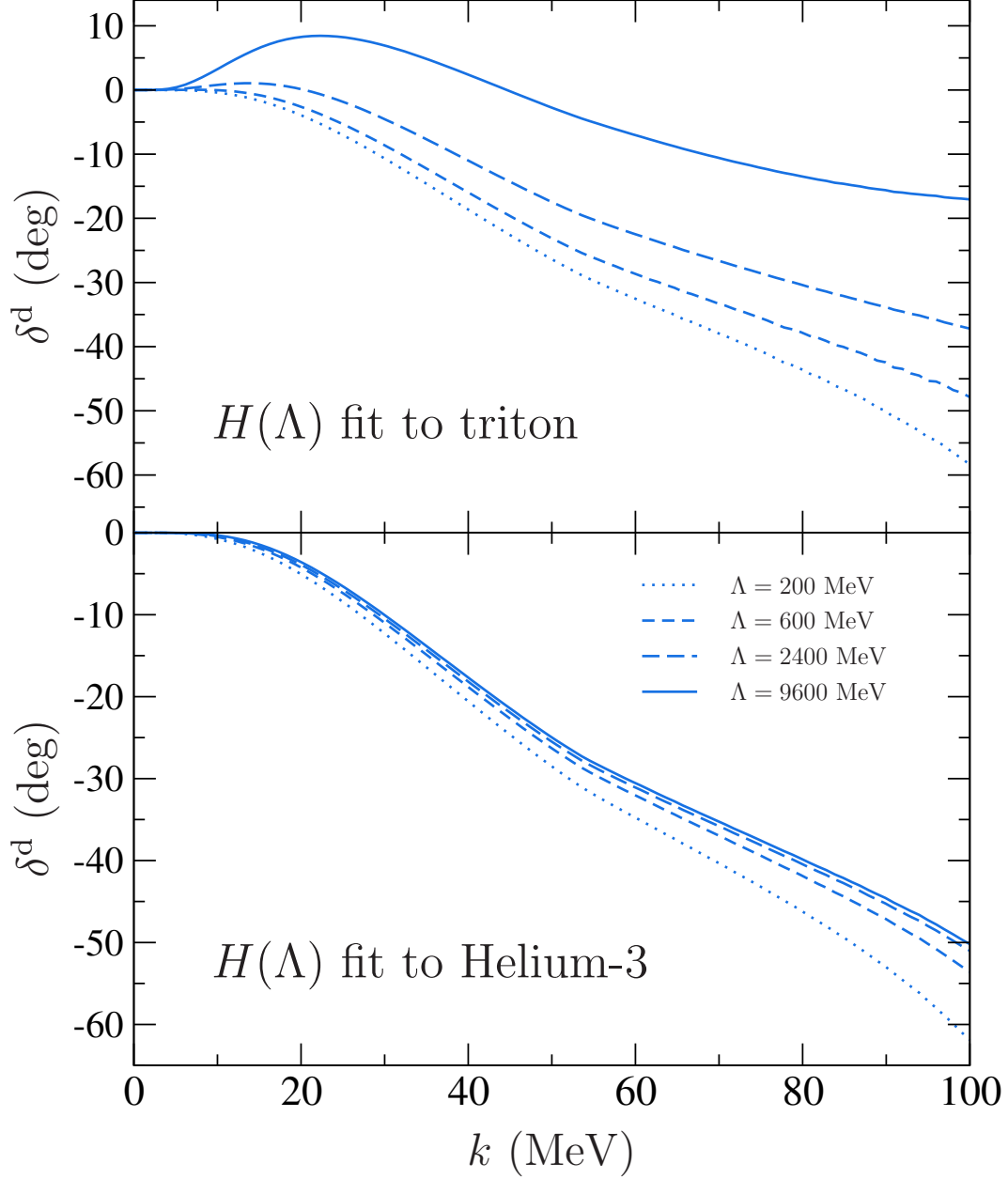


FIG. 19: NLO p - d scattering phase shifts for large cutoffs obtained using Eq. (64). Upper panel: $H(\Lambda)$ fit to reproduce triton binding energy in the n - d system. Lower panel: $H(\Lambda)$ fit to reproduce ${}^3\text{He}$ binding energy in the p - d system.

between the effects of the individual Coulomb diagrams.

A similar effect occurs in the quartet channel. In this case we have additionally calculated the result with the bubble diagram still approximated, but the box diagram¹⁶ already included. Overall, the results from the individual calculations shown in Fig. 21 differ now

¹⁶ Note that the triangle diagram does not appear in the quartet channel since there are never two protons in the intermediate dibaryon.

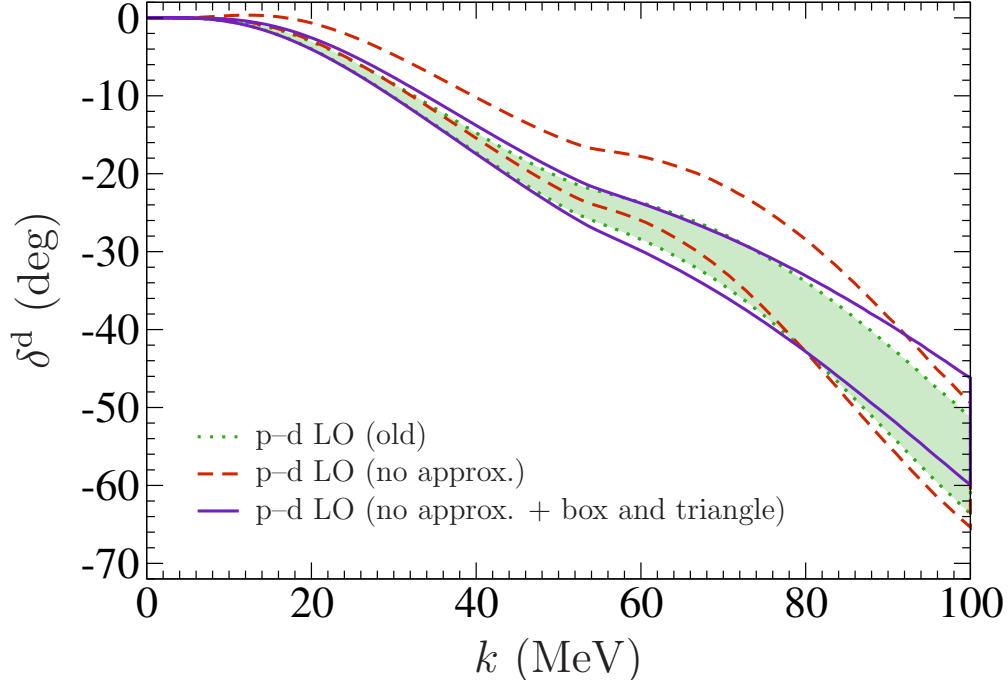


FIG. 20: Leading order p - d doublet channel S-wave scattering phase shifts as functions of the center-of-mass momentum k . Dotted curve: old result from Ref. [26]. Dashed curve: result without approximating the bubble diagram. Solid curve: same as dashed curve with additional Coulomb diagrams (box and triangle) included. Error bands generated by cutoff variation within 200–600 MeV.

not so much at low center-of-mass momenta, but quite substantially above the deuteron break-up threshold ($k \gtrsim 52$ MeV). Since the error bands would be as narrow as in Fig. 10 of Ref. [26] and are not essential for what we want to show here, we have used a single cutoff $\Lambda = 140$ MeV to generate the curves.

The cancellation between the two effects is particularly striking here: the result obtained with both the bubble-diagram approximation turned off and the box diagram included at the same time (solid curve) is almost identical to the old result (dotted curve). We have shown here the results at N²LO where above the breakup threshold the effect of the cancellation is in fact somewhat larger than the expected uncertainty from the EFT expansion at this order. The same pattern is found also at lower orders calculations.

Altogether, these findings cast some doubt on the Coulomb power counting as discussed in Section II C. In particular, the good agreement of the N²LO quartet-channel phase shifts with experimental data that was found based on this counting scheme already in Ref. [23] appears now to be somewhat accidental, at least at higher energies. Based on the findings obtained here we propose that instead of using the old counting it might be better—also in the scattering regime—to simply include already at leading order all $\mathcal{O}(\alpha)$ Coulomb diagrams if they are not, like Fig. 3(d), formally range corrections. At the same time, as already alluded to below Eq. (35), one should not use the approximation for the bubble diagram because it has no physical justification and turns out to have a more significant impact on the result than naïvely expected.

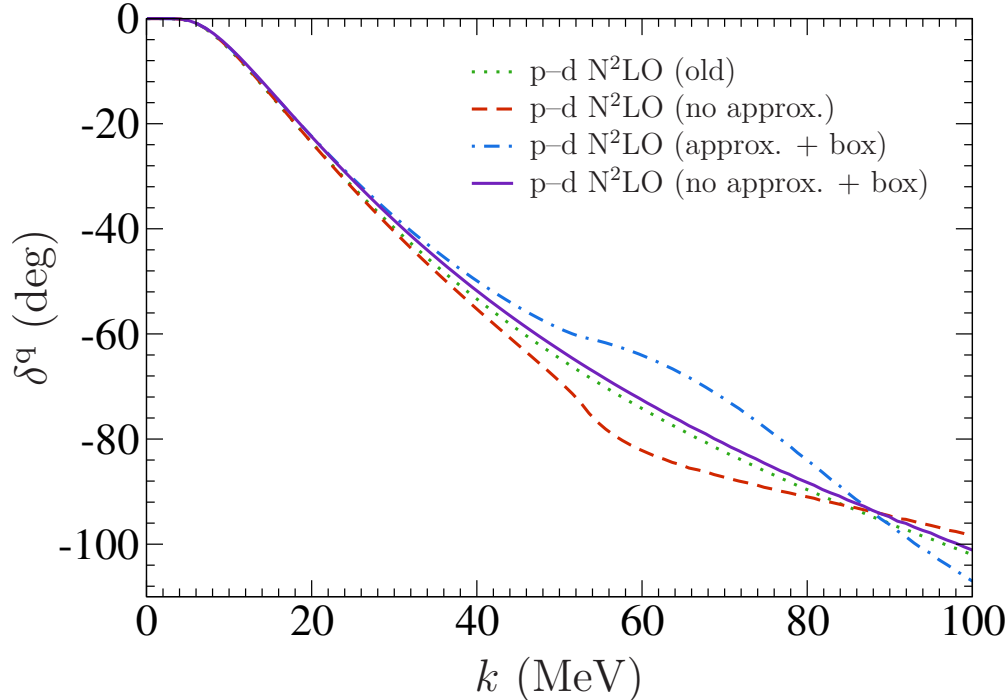


FIG. 21: $N^2\text{LO}$ p - d quartet channel S-wave scattering phase shifts as functions of the center-of-mass momentum k . Dotted curve: old result from Ref. [26]. Dashed curve: result without approximating the bubble diagram. Dash-dotted curve: result with the additional Coulomb box diagram box included (but the bubble diagram still approximated). Solid curve: same as dash-dotted curve, but without approximating the bubble diagram. All curves were calculated at a cutoff $\Lambda = 140$ MeV.

This new scheme¹⁷ has the advantage of being much more straightforward and at the same time completely consistent throughout both the scattering and the bound-state regime. The price to be paid for this is that the calculations to be carried out are quite a bit more involved. With suitable adaptive integration routines to carry out the S-wave projections of the Coulomb diagrams numerically, however, the integral equations can still be solved on ordinary desktop computers.

VII. HIGHER-ORDER COULOMB CONTRIBUTIONS

Having concluded that the original Coulomb counting scheme should be modified raises the question how large higher-order contributions (in α) really are. Very close to the zero-momentum threshold one would naïvely think them to be quite important.

¹⁷ We would like to emphasize here that the new scheme does not imply to do strict perturbation theory in α . Since we want to calculate scattering at low energies, the included Coulomb diagrams are still iterated nonperturbatively to all orders, which means that the perturbation expansion up to $\mathcal{O}(\alpha)$ is applied to the *kernels* used in the Lippmann–Schwinger equations.

A. Diagrams with full off-shell Coulomb T-matrix

Since the Coulomb interaction is strongest directly at threshold, the scattering calculation should be a good testing ground for checking the influence of higher-order Coulomb diagrams that we have not taken into account so far. Rather than simply including $\mathcal{O}(\alpha^2)$ diagrams (with two Coulomb-photon exchanges) to estimate the effect of higher-order terms, we adopt the approach of Ando and Birse [24] and directly include the full off-shell Coulomb T-matrix in the diagrams. Effectively, this resums all subsequent Coulomb-photon exchanges for a given topology. The resulting diagrams are shown in Fig. 22.

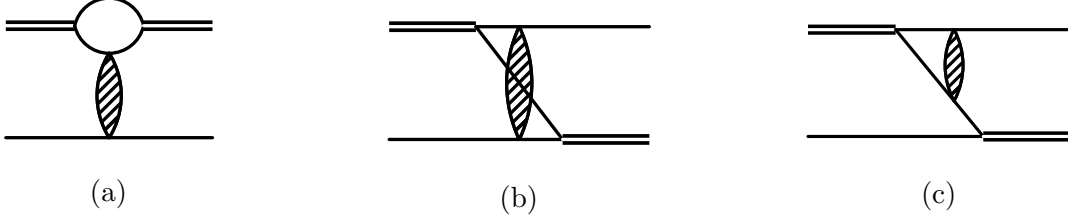


FIG. 22: Diagrams involving the full off-shell Coulomb T-matrix (indicated by the blob).

In Ref. [24], Ando and Birse only consider the bound-state regime and argue that the finite extent of the wave functions helps to regularize the Coulomb singularity and thus use an unscreened interaction. Since we cannot apply this approach in the scattering regime, we use here a “partially screened” Coulomb T-matrix $T_{C,\lambda}$ that is described in more detail in Appendix B. Going back to an approach by Gorshkov [55, 56], $T_{C,\lambda}$ is defined by the operator equation

$$\hat{T}_{C,\lambda} = \hat{V}_{C,\lambda} + \hat{V}_{C,\lambda} \hat{G}_0^{(+)} \hat{T}_C, \quad (78)$$

where \hat{T}_C is the exact unscreened Coulomb T-matrix and $\hat{G}_0^{(+)}$ is the free two-particle resolvent (Green’s function). In Appendix B we show that very similar to the unscreened Coulomb T-matrix, $T_{C,\lambda}$ can be expressed in terms of hypergeometric functions as

$$T_{C,\lambda}(k; \mathbf{p}, \mathbf{q}) = V_C(\mathbf{p}, \mathbf{q}) \left\{ 1 - \Delta_\lambda^{-1} \left[{}_2F_1(1, i\eta, 1 + i\eta; X_\lambda^-) - {}_2F_1(1, i\eta, 1 + i\eta; X_\lambda^+) \right] \right\}, \quad (79)$$

with Δ_λ and X_λ^\pm as defined in Eqs. (B40) and (B41), respectively.

We assume that using $T_{C,\lambda}$ in the p - d integral equations gives an appropriate description for small photon masses λ because in the limit $\lambda \rightarrow 0$, $T_{C,\lambda}$ converges to the exact (unscreened) Coulomb T-matrix T_C .

1. Bubble diagram

The most important contribution is again given by the “full bubble diagram” shown in Fig. 22a. Its spin- and isospin structure is exactly the same as for the leading expression with just a single Coulomb-photon exchange. However, the loop integral, which before could

be evaluated analytically, now has the more complicated form

$$\mathcal{I}_{\text{bubble}}^{\text{full}}(E; \mathbf{k}, \mathbf{p}) = \int_0^\infty dq q^2 T_{C,\lambda}(i\sqrt{3q^2/4 - M_N E}; \mathbf{k}, \mathbf{p}) \times \int_{-1}^1 d\cos\theta' \int_0^{2\pi} \frac{d\phi'}{a(b + c \cdot \cos\phi')} \quad (80)$$

with

$$a = k^2 + kq \cos\theta' + q^2 - M_N E, \quad (81a)$$

$$b = p^2 + pq \cos\theta \cos\theta' + q^2 - M_N E, \quad (81b)$$

$$c = pq \sin\theta \sin\theta'. \quad (81c)$$

Here, as in Eqs. (65) and (66a), θ is the angle between the vectors \mathbf{k} and \mathbf{p} , whereas θ' denotes the angle between \mathbf{k} and the loop momentum \mathbf{q} , and the azimuthal angle ϕ' enters through rewriting the angle between \mathbf{p} and \mathbf{q} . It can be integrated over analytically with the result

$$\int_0^{2\pi} \frac{d\phi'}{b + c \cdot \cos\phi'} = \frac{2\pi}{\sqrt{b^2 - c^2}} \quad (82)$$

for $b > c$, which, according to Eqs. (81) is fulfilled for the scattering-length calculation. Only above the deuteron breakup threshold, where the energy E is positive, one would have to be more careful at this point.

Setting

$$\cos\theta' \equiv x \Rightarrow \sin\theta' = \sqrt{1 - x^2}, \quad (83)$$

the remaining angular integral has the form

$$\int_{-1}^1 \frac{dx}{(A + B \cdot x)\sqrt{C + D \cdot x + E \cdot x^2}} \quad (84)$$

with

$$A = k^2 + q^2 - M_N E, \quad (85a)$$

$$B = kq, \quad (85b)$$

$$C = (p^2 + q^2 - M_N E)^2 - p^2 q^2 (1 - \cos^2\theta) \quad (85c)$$

$$D = (p^2 + q^2 - M_N E) \times 2pq \cos\theta \quad (85d)$$

$$E = p^2 q^2. \quad (85e)$$

Using integration by parts, this can be done analytically. The final result for the full-bubble kernel function is then¹⁸

$$K_{\text{bub}}^{(\text{full})}(E; k, p) = -\frac{M_N}{2\pi^2} \times \frac{1}{2} \int_{-1}^1 d\cos\theta \mathcal{I}_{\text{bubble}}^{\text{full}}(E; \mathbf{k}, \mathbf{p}) \quad (86)$$

¹⁸ Note that the expression in Eq. (87) does not directly reduce to $\mathcal{I}_{\text{bubble}}$ as defined in Eq. (33) when the Coulomb T-matrix is replaced with a single photon exchange. Rather, in that limit, the kernel function $K_{\text{bub}}^{(\text{full})}(E; k, p)$ goes over into the LO-part of Eq. (37), including the overall prefactor $-\alpha M_N$.

with

$$\begin{aligned} \mathcal{I}_{\text{bubble}}^{\text{full}}(E; \mathbf{k}, \mathbf{p}) &= \int_0^\infty dq q^2 T_{C,\lambda}\left(i\sqrt{3q^2/4 - M_N E}; \mathbf{k}, \mathbf{p}\right) \\ &\times \frac{1}{\sqrt{F}} \left[\log\left(\frac{A+B}{A-B}\right) - \log\left(\frac{B(2C+D) - A(D+2E) + 2\sqrt{F}\sqrt{C+E+D}}{B(2C-D) - A(D-2E) + 2\sqrt{F}\sqrt{C+E-D}}\right) \right], \end{aligned} \quad (87)$$

where in addition to Eqs. (85) we have defined

$$F = B^2 C + A^2 E - ABD. \quad (88)$$

The remaining momentum integral and the S-wave projection in Eq. (86) have to be carried out numerically.

Unfortunately, similar tricks cannot be used to simplify the expression for the full box and triangle diagrams shown in Figs. 22b and c. In those cases, the Coulomb T-matrix depends non-trivially on the loop momentum, which means that the angular integrations can no longer be carried out analytically.

2. Box diagram

The full box diagram, Fig. 22b, can be written as

$$K_{\text{box}}^{(\text{full})}(E; k, p) = -\frac{M_N}{8\pi^3} \times \frac{1}{2} \int_{-1}^1 d\cos\theta \mathcal{I}_{\text{box}}^{\text{full}}(E; \mathbf{k}, \mathbf{p}). \quad (89)$$

The loop integral is

$$\mathcal{I}_{\text{box}}^{\text{full}}(E; \mathbf{k}, \mathbf{p}) = \int d^3q \frac{T_{C,\lambda}\left(i\sqrt{3q^2/4 - M_N E}; \mathbf{k} - \mathbf{q}, -\mathbf{p}\right)}{(\mathbf{q}^2 - \mathbf{q} \cdot \mathbf{k} + \mathbf{k}^2 - M_N E)(\mathbf{q}^2 - \mathbf{q} \cdot \mathbf{p} + \mathbf{p}^2 - M_N E)} \quad (90)$$

with

$$\int d^3q = \int_0^\infty dq q^2 \int_0^\pi d\theta' \int_0^{2\pi} d\phi' \quad (91)$$

and the angles

$$\mathbf{q} \cdot \mathbf{k} = qk \cos\theta', \quad (92a)$$

$$\mathbf{q} \cdot \mathbf{p} = pq(\cos\theta \cos\theta' + \sin\theta \sin\theta' \cos\phi'). \quad (92b)$$

Recall that θ is the angle between \mathbf{k} and \mathbf{p} . As mentioned above, all four integrations in this expression (three angles plus the loop momentum) have to be carried out numerically.

B. Comparison of quartet-channel phase shifts

Performing the integrals for the full bubble diagram as given in Eq. (86) is still feasible with standard numerical quadrature rules. For the four-dimensional integration necessary to evaluate the full box diagram, however, we use the Vegas Monte-Carlo algorithm implemented in the CUBA library [57]. To evaluate the Coulomb T-matrix we use the expression

in terms of hypergeometric functions given in Eq. (79), which can be implemented efficiently with the fast routines for ${}_2F_1$ from Ref. [58].

Results for leading-order quartet-channel phase shifts at $\Lambda = 140$ MeV are shown in Fig. 23. The plot demonstrates that for scattering momenta below the deuteron breakup threshold, higher-order Coulomb corrections clearly are negligible. Only for center-of-mass momenta larger than about 35 MeV does one see noticeable differences from the result with only the leading $\mathcal{O}(\alpha)$ bubble and box diagrams included (solid curve in Fig. 23). One can understand this by noting that the energy flowing into $T_{C,\lambda}$ is always given by $3q^2/4 - M_N E$, where q is the loop momentum. Since in the scattering regime $E = 3k^2/(4M_N) - \gamma_d^2/M_N$, this can only be close to zero if $k \approx \sqrt{4/3}\gamma_d$. For energies above the breakup threshold the full Coulomb T-matrix is expected to have a stronger influence [51, 52], but in that regime the numerical calculation is even more challenging (due to imaginary parts opening up) and has not been performed yet. We can conclude, however, that for p - d scattering at very low energies it is indeed valid to only include $\mathcal{O}(\alpha)$ Coulomb diagrams in the integral equation kernels.

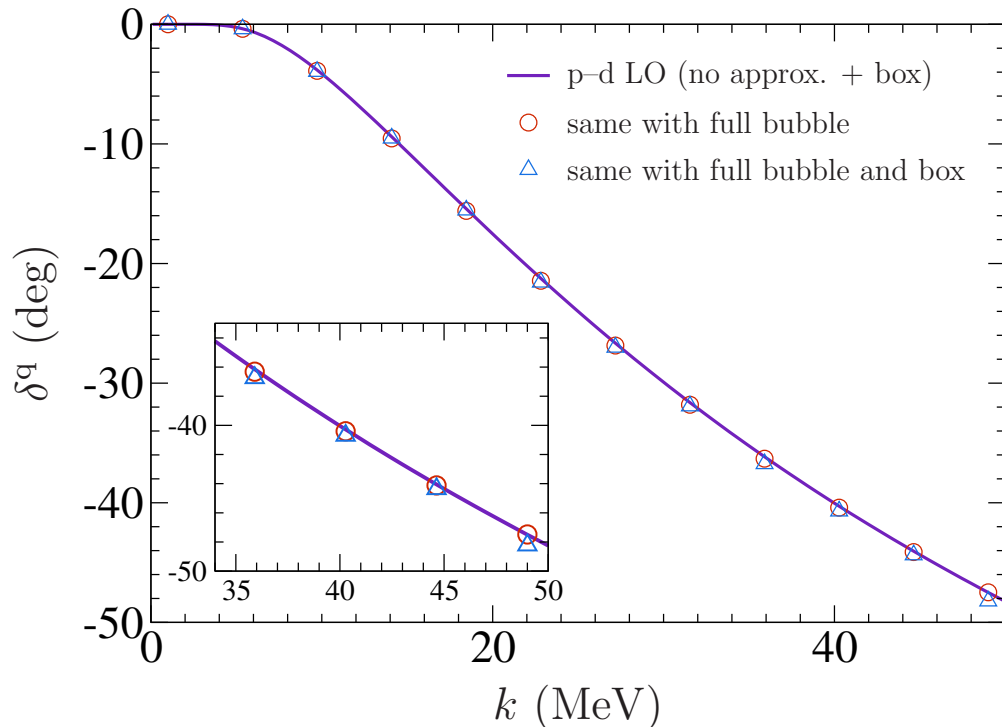


FIG. 23: Leading order p - d quartet channel S-wave scattering phase shifts as functions of the center-of-mass momentum k . Solid curve: calculation with ordinary bubble (no approximation) and box diagrams. Circles: calculation with full bubble diagram. Triangles: calculation with full bubble and box diagrams. All curves were calculated at a cutoff $\Lambda = 140$ MeV. See text for more details.

VIII. SUMMARY AND OUTLOOK

In this paper we have studied several aspects of the proton–deuteron system in pionless effective field theory. In the bound-state regime, we have amended our previous [26] perturbative calculation of the ${}^3\text{He}$ – ${}^3\text{H}$ binding energy difference and additionally performed a nonperturbative calculation of the ${}^3\text{He}$ binding energy that agrees very well with the result obtained by Ando and Birse [24] although we have only used Coulomb photons to include electromagnetic effects. Furthermore, at leading order both the perturbative and the nonperturbative calculation give results that are, within their respective uncertainties, in good agreement with the experimental value for the ${}^3\text{He}$ binding energy.

At next-to-leading order, the results of both calculations exhibit a strong cutoff dependence, indicating that the calculation is not renormalized properly. We have analyzed this situation by studying the ultraviolet behavior of the diagrams entering in the calculation and argued that this provides evidence for a new three-body counterterm being necessary to renormalize the charged doublet-channel system at NLO. Indeed such a term has been identified in Ref. [28].

Re-examining the doublet-channel scattering calculation we find that the phase shifts presented in Ref. [26] turn out not to converge when the cutoff in the calculation is chosen very large. Consistent with a new counterterm entering at NLO, this cutoff dependence however goes away when one refits a single three-nucleon force to reproduce the experimental ${}^3\text{He}$ binding energy. Since the modified fitting of the three-nucleon force requires using the same equation structure in the bound-state and scattering regime, we have critically reviewed the Coulomb power counting of Rupak and Kong [23] and come to the conclusion that it might be better to simply include all Coulomb diagrams of a given order in α . This approach is simpler and more consistent because it treats the scattering and bound-state regimes on an equal footing.

Finally, we have shown that higher-order (in α) Coulomb contributions can safely be neglected in quartet-channel p – d scattering. With that, it is interesting to proceed further towards the zero-energy threshold and also calculate Coulomb-modified scattering lengths. A first step in that direction has already been made in Ref. [27]. Recently, a fully perturbative calculation of the quartet-channel scattering length up to N²LO has been presented in Ref. [40]. In the future, we plan on analyzing that calculation in more detail and furthermore to extend the approach also to the doublet channel.

Acknowledgments

We thank Dean Lee, Daniel R. Phillips, Jared Vanasse and U. van Kolck for useful discussions, Martin Hoferichter for help with the calculation of the box diagram, and Philipp Hagen for suggestions concerning the trimer Z -factor. HWG is particularly indebted to the Nuclear Theory groups at U. Bonn and FZ Jülich for their hospitality during his Sabbatical stay. S.K. furthermore thanks the “Studienstiftung des deutschen Volkes” and the Bonn-Cologne Graduate School of Physics and Astronomy for their support. This research was supported in part by the NSF under Grant No. PHY–1306250 and by the NUCLEI SciDAC Collaboration under DOE Grant DE-SC0008533 (SK), by the DFG through SFB/TR 16 “Subnuclear structure of matter”, by the BMBF under grant 05P12PDFTE, by the Helmholtz Association under contract HA216/EMMI (HWH, SK), as well as by the US-Department of Energy under contract DE-FG02-95ER-40907, by the Deutsche Forschungsgemeinschaft and the

National Natural Science Foundation of China through funds provided to the Sino-German CRC 110 ‘‘Symmetries and the Emergence of Structure in QCD’’, and by the EPOS network of the European Community Research Infrastructure Integrating Activity ‘‘Study of Strongly Interacting Matter HadronPhysics3’’ (HWG).

Appendix A: T-matrix factorization and wave function normalization

We discuss here in some detail the factorization of the \mathcal{T} -matrix given in Eq. (46) and the normalization condition (50) for the trinucleon wave functions. The latter has already been discussed in the appendix of Ref. [26]. The following material is based on an extension of those results, originally presented in Ref. [27]. We point out again that nontrivial normalization conditions for bound-state wave functions arising from energy-dependent interactions have been known for a long time [49]. The purpose of this appendix is to present a self-contained and rather pedagogical derivation, originally based on that given in Lurie’s textbook [59].

1. Bethe–Salpeter equation

As in Ref. [26] we consider a simplified nucleon–deuteron system where we neglect the spin-singlet dibaryon for the moment. Our starting point is the Bethe–Salpeter in momentum space,

$$G(k, p; P) = G_0(k, p; P) + \int \frac{d^4 q}{(2\pi)^4} \int \frac{d^4 q'}{(2\pi)^4} G(k, q; P) K(q, q'; P) G_0(q', p; P), \quad (\text{A1})$$

where G denotes the full two-body nucleon–deuteron Green’s function (related directly to the S-matrix). G_0 describes the momentum-conserving free propagation of the individual particles,

$$G_0(k, p; P) = (2\pi)^4 \delta^{(4)}(k - p) \cdot \Delta_d(\eta_d P + p) \Delta_N(\eta_N P - p) \quad (\text{A2})$$

with the total four-momentum P and the mass ratios $\eta_{N,d}$ fulfilling $\eta_d + \eta_N = 1$. The interaction kernel K is given by the (spin/isospin and S-wave projected) one-nucleon-exchange diagram,

$$K(k_0, \mathbf{k}, p_0, \mathbf{p}; E) = \frac{-iy_d^2/2}{\eta_d E - \eta_N E + k_0 + p_0 - \frac{(\mathbf{k} + \mathbf{p})^2}{2M_N} + i\epsilon}, \quad (\text{A3})$$

In order to describe the real doublet-channel system of Sec. IV, all quantities defined above become matrices in channel space and one has to include the three-nucleon contact interaction in K .

Assuming the existence of a trinucleon bound state (the triton in our current toy model) at an energy $E = -E_B < 0$, one can show that [27, 59]

$$G(k, p; P) = i \frac{\psi_{B\mathbf{P}}(p) \psi_{B\mathbf{P}}^\dagger(k)}{E + E_B + i\epsilon} + \text{terms regular at } P_0 = E = -E_B, \quad (\text{A4})$$

i.e. G factorizes at the bound state pole. Inserting the above factorization into Eq. (A1) and multiplying by $(E + E_B)$ we find the homogeneous Bethe–Salpeter equation

$$\int \frac{d^4 q}{(2\pi)^4} [G_0^{-1}(q, p; P) - K(q, p; P)] \psi_{B\mathbf{P}}(q) = 0 \quad (\text{A5})$$

after taking the limit $E \rightarrow -E_B$ and cancelling non-zero factors. Equivalently, we can also obtain this in the form

$$\psi_{B\mathbf{P}}(p) = \Delta_d(\eta_d P + p) \Delta_N(\eta_N P - p) \cdot \int \frac{d^4 q}{(2\pi)^4} K(q, p; P) \psi_{B\mathbf{P}}(q) \quad (\text{A6})$$

from Eq. (A1).

2. Three-dimensional reduction

We now consider a bound state at rest, $P = (-E_B, \mathbf{0})$, and define the *amputated wave function*

$$\mathcal{B}(p_0, \mathbf{p}) = \psi_{B\mathbf{0}}(p_0, \mathbf{p}) \cdot [\Delta_d(-\eta_d E_B + p_0, \mathbf{p})]^{-1} \cdot [\Delta_N(-\eta_N E_B - p_0, \mathbf{p})]^{-1}, \quad (\text{A7})$$

which fulfills the equation

$$\mathcal{B}(p_0, \mathbf{p}) = \int \frac{d^4 q}{(2\pi)^4} K(q, p; -E_B) \Delta_d(-\eta_d E_B + q_0, \mathbf{q}) \Delta_N(-\eta_N E_B - q_0, \mathbf{q}) \mathcal{B}(q_0, \mathbf{q}). \quad (\text{A8})$$

Carrying out the dq_0 integration picks up the residue from the nucleon propagator pole at $q_0 = -\eta_N E_B - \mathbf{q}^2/(2M_N) + i\varepsilon$. From the resulting right-hand side of Eq. (A8) we then find that the function

$$\mathcal{B}(\mathbf{p}) \equiv \mathcal{B}\left(-\eta_N E_B - \frac{\mathbf{p}^2}{2M_N}, \mathbf{p}\right) \quad (\text{A9})$$

fulfills the equation

$$\mathcal{B}(\mathbf{p}) = \int \frac{d^3 q}{(2\pi)^3} K\left(\eta_N E - \frac{\mathbf{q}^2}{2M_N}, \mathbf{k}, \eta_N E - \frac{\mathbf{p}^2}{2M_N}, \mathbf{p}; E\right) \Delta_d\left(-E_B - \frac{\mathbf{q}^2}{2M_N}, \mathbf{q}\right) \mathcal{B}(\mathbf{q}). \quad (\text{A10})$$

For future reference we also define the wave function

$$\phi(\mathbf{p}) = \int \frac{dp_0}{2\pi} \psi(p_0, \mathbf{p}), \quad (\text{A11})$$

for which from Eq. (A7) one immediately finds that

$$\phi(\mathbf{p}) = \Delta_d\left(-E_B - \frac{\mathbf{p}^2}{2M_N}, \mathbf{p}\right) \mathcal{B}(\mathbf{p}). \quad (\text{A12})$$

3. Operator formalism

To see what exactly the factorization Eq. (A4) implies for the \mathcal{T} -matrix we now introduce an abstract operator notation. The Bethe–Salpeter equation (A1) can be written as

$$G = G_0 + GKG_0 = G_0 + G_0KG, \quad (\text{A13})$$

where the middle and the right-hand side are equivalent.¹⁹ Assuming again the existence of a bound state with energy $E = -E_B$, we have the factorization

$$G \sim i \frac{|\psi\rangle\langle\psi|}{E + E_B} \quad \text{for } E \rightarrow -E_B, \quad (\text{A14})$$

as given explicitly in Eq. (A4). Inserting this into Eq. (A13), multiplying by $(E + E_B)$, and acting on $|\psi\rangle$, we obtain the homogeneous equation

$$|\psi\rangle = G_0 K |\psi\rangle \quad (\text{A15})$$

after taking the limit $E \rightarrow -E_B$ and using that G_0 is regular for $E \rightarrow -E_B$. This is, of course, just Eq. (A6). Note that all the operators here are in general functions of the total energy, $G = G(E)$, $K = K(E)$, etc., but that for the sake of notational convenience we have not written out this dependence explicitly.

4. Lippmann–Schwinger equation

Defining the T-matrix operator T via the relation

$$KG = TG_0, \quad (\text{A16})$$

we can rewrite Eq. (A13) in the form

$$G = G_0 + G_0 T G_0. \quad (\text{A17})$$

Inserting this into both sides of the original Eq. (A13), we get

$$G_0 + G_0 T G_0 = G_0 + G_0 K G_0 + G_0 K G_0 T G_0. \quad (\text{A18})$$

After cancelling the common term G_0 and multiplying through by G_0^{-1} on both sides, we arrive at the familiar Lippmann–Schwinger equation

$$T = K + K G_0 T. \quad (\text{A19})$$

The above relations will be used in Sec. A6 to find the proper factorization of the \mathcal{T} -matrix. First, however, we consider again the homogeneous equation and derive the normalization condition in the operator formalism.

5. Normalization condition

Going back momentarily to the explicit momentum-space basis we again set $P = (-E_B, \mathbf{0})$ and define a reduced two-body propagator \tilde{G} that only depends on the relative three-momenta \mathbf{k} and \mathbf{p} by integration over the energies:

$$\tilde{G}(\mathbf{k}, \mathbf{p}; -E_B) = \int \frac{dk_0}{2\pi} \int \frac{dp_0}{2\pi} G(k, p; P). \quad (\text{A20})$$

¹⁹ This can be seen, for example, by iterating both versions and noting that the results are the same.

By the definition (A11), this implies

$$\tilde{G} \sim i \frac{|\phi\rangle\langle\phi|}{E + E_B} \text{ for } E \rightarrow -E_B. \quad (\text{A21})$$

From Eq. (A13) we get

$$\tilde{G} = \tilde{G}_0 + \widetilde{G_0 K G} = \tilde{G}_0 \left(\mathbf{1} + \tilde{G}_0^{-1} \widetilde{G_0 K G} \right) \quad (\text{A22})$$

and hence

$$\tilde{G}^{-1} = \left(\mathbf{1} + \tilde{G}_0^{-1} \widetilde{G_0 K G} \right)^{-1} \tilde{G}_0^{-1}. \quad (\text{A23})$$

We now define

$$\tilde{G}^{-1} - \tilde{G}_0^{-1} \equiv -\tilde{V} \quad (\text{A24})$$

and find

$$\tilde{G} = \tilde{G} \left(\tilde{G}_0^{-1} - \tilde{V} \right) \tilde{G}. \quad (\text{A25})$$

Inserting Eq. (A21) and using l'Hôpital's rule to evaluate the limit $E \rightarrow -E_B$, we readily derive the normalization condition

$$i \langle \phi | \frac{d}{dE} \left(\tilde{G}_0^{-1} - \tilde{V} \right) | \phi \rangle \Big|_{E=-E_B} = 1, \quad (\text{A26})$$

where $\tilde{V} = \tilde{G}_0^{-1} - \tilde{G}^{-1}$, *cf.* Eq. (A24). A straightforward calculation shows that

$$\tilde{G}_0^{-1}(\mathbf{k}, \mathbf{p}; E) = (2\pi)^3 \delta^{(3)}(\mathbf{k} - \mathbf{p}) \cdot \left[\Delta_d \left(E - \frac{\mathbf{p}^2}{2M_N}, \mathbf{p} \right) \right]^{-1}, \quad (\text{A27})$$

and we also see that $|\mathcal{B}\rangle = \tilde{G}_0^{-1}|\phi\rangle$. For the \tilde{V} defined in Eq. (A24) we get

$$\tilde{V} = \tilde{G}_0^{-1} - \left(\mathbf{1} + \tilde{G}_0^{-1} \widetilde{G_0 K G} \right)^{-1} \tilde{G}_0^{-1} = \tilde{G}_0^{-1} - \left[\sum_{n=0}^{\infty} \left(-\tilde{G}_0^{-1} \widetilde{G_0 K G} \right)^n \right] \tilde{G}_0^{-1}. \quad (\text{A28})$$

Furthermore, iterated application of the Bethe–Salpeter equation (A13) yields

$$\widetilde{G_0 K G} = \widetilde{G_0 K G_0} + G_0 \widetilde{K G_0 K G_0} + \dots, \quad (\text{A29})$$

such that we have a double expansion in Eq. (A28). We write

$$\tilde{V} \equiv \sum_{n=0}^{\infty} \tilde{V}_n = \underbrace{\tilde{G}_0^{-1} - \tilde{G}_0^{-1}}_{\tilde{V}_{0=0}} + \underbrace{\tilde{G}_0^{-1} \widetilde{G_0 K G_0} \tilde{G}_0^{-1}}_{\tilde{V}_1} + \dots, \quad (\text{A30})$$

where the index indicates the number of insertions of K . This expression is turns out to be far simpler than it looks since all \tilde{V}_n with $n > 0$ actually vanish. This can be seen by induction if one uses the relation

$$\dots \widetilde{G_0 G_0^{-1} G_0} \dots = \dots \widetilde{G_0} \dots \quad (\text{A31})$$

More details about this and a proof of Eq. (A31) can be found in Refs. [26, 27]. The final result is simply

$$\begin{aligned}\widetilde{V}(\mathbf{k}, \mathbf{p}; E) &= K \left(\eta_N E - \frac{\mathbf{k}^2}{2M_N}, \mathbf{k}, \eta_N E - \frac{\mathbf{p}^2}{2M_N}, \mathbf{p}; E \right) \\ &= \frac{iM_N y_d^2}{2} \cdot \frac{1}{\mathbf{k}^2 + \mathbf{k} \cdot \mathbf{p} + \mathbf{p}^2 - M_N E - i\varepsilon}.\end{aligned}\tag{A32}$$

The only remaining step is to derive from Eq. (A26) the normalization condition for trinucleon wave functions $\mathcal{B}(\mathbf{p})$. This can be done most clearly by first establishing the connection between the quantities defined here and the \mathcal{T} -matrix elements used in the main part of this paper. We are now finally in a position to do that.

6. Factorization of the T-matrix

Comparing Eqs. (A10) and (A32) with the interaction as given in Section III already suggests that there is a direct correspondence between the states $\mathcal{B}(\mathbf{p})$ introduced here and the trinucleon wave functions of Sec. IV. For the T operator introduced in Eq. (A16) we find from Eq. (A18) that

$$\widetilde{G}_0 \widetilde{T} G_0 = \widetilde{G}_0 \widetilde{K} G_0 + G_0 \widetilde{K} \widetilde{G}_0 \widetilde{T} G_0.\tag{A33}$$

Applying Eq. (A31) to the second term on the right-hand side gives

$$G_0 \widetilde{K} \widetilde{G}_0 \widetilde{T} G_0 = \widetilde{G}_0 \widetilde{K} G_0 \widetilde{G}_0^{-1} \widetilde{G}_0 \widetilde{T} G_0.\tag{A34}$$

Inserting into this the identity in the form

$$\mathbf{1} = \widetilde{G}_0 \widetilde{G}_0^{-1}\tag{A35}$$

and multiplying Eq. (A33) with \widetilde{G}_0^{-1} from both sides we find that

$$\widetilde{G}_0^{-1} \widetilde{G}_0 \widetilde{T} G_0 \widetilde{G}_0^{-1} = \left[\widetilde{G}_0^{-1} \widetilde{G}_0 \widetilde{K} G_0 \widetilde{G}_0^{-1} \right] \widetilde{G}_0 \left[\widetilde{G}_0^{-1} \widetilde{G}_0 \widetilde{T} G_0 \widetilde{G}_0^{-1} \right],\tag{A36}$$

where from the discussion in Section A 5 we see that the interaction is the same as in the normalization condition:

$$\widetilde{G}_0^{-1} \widetilde{G}_0 \widetilde{K} G_0 \widetilde{G}_0^{-1} = \widetilde{V}.\tag{A37}$$

Comparing this now with the integral equations in Sec. III, we can conclude that the \mathcal{T} -matrix defined there is

$$i\mathcal{T}(E; \mathbf{k}, \mathbf{p}) = \langle \mathbf{k} | \widetilde{G}_0^{-1} \widetilde{G}_0 \widetilde{T} G_0 \widetilde{G}_0^{-1} | \mathbf{p} \rangle,\tag{A38}$$

where all operators are of course functions of the energy E .

As $E \rightarrow -E_B$ we now have, using Eq. (A17) and noting that the bound state cannot be in G_0 since it has to arise from the interaction,

$$\widetilde{G}_0^{-1} \widetilde{G}_0 \widetilde{T} G_0 \widetilde{G}_0^{-1} \rightarrow \widetilde{G}_0^{-1} \widetilde{G} \widetilde{G}_0^{-1} + \text{regular terms} = i \frac{\widetilde{G}_0^{-1} |\phi\rangle \langle \phi| \widetilde{G}_0^{-1}}{E + E_B} + \text{regular terms},\tag{A39}$$

where the second identity follows from Eq. (A21). Now, according to Eqs. (A12) and (A27) we have

$$|\phi\rangle = \tilde{G}_0|\mathcal{B}\rangle \iff |\mathcal{B}\rangle = \tilde{G}_0^{-1}|\phi\rangle, \quad (\text{A40})$$

which implies

$$\langle\mathcal{B}| = \langle\phi|(\tilde{G}_0^{-1})^\dagger. \quad (\text{A41})$$

But—up to a delta function— \tilde{G}_0^{-1} is just the deuteron propagator Δ_d which, from Eq. (9) we find to be a purely imaginary quantity.²⁰ Hence,

$$(\tilde{G}_0^{-1})^\dagger = -\tilde{G}_0^{-1}, \quad \text{for } E < 0 \quad (\text{A42})$$

and

$$\tilde{G}_0^{-1}\widetilde{G_0TG_0}\tilde{G}_0^{-1} = -i\frac{|\mathcal{B}\rangle\langle\mathcal{B}|}{E + E_B} + \text{regular terms as } E \rightarrow -E_B. \quad (\text{A43})$$

For the \mathcal{T} -matrix we then find from Eq. (A38) that

$$\mathcal{T}(E; \mathbf{k}, \mathbf{p}) = -\frac{\mathcal{B}^\dagger(\mathbf{k})\mathcal{B}(\mathbf{p})}{E + E_B} + \text{regular terms as } E \rightarrow -E_B. \quad (\text{A44})$$

Finally, for the normalization condition (A26) written in terms of the states $|\mathcal{B}\rangle$ we analogously find

$$-i\langle\mathcal{B}|\tilde{G}_0\left[\frac{d}{dE}\left(\tilde{G}_0^{-1} - \tilde{V}\right)\right]\tilde{G}_0|\mathcal{B}\rangle\Big|_{E=-E_B} = 1. \quad (\text{A45})$$

This can be directly translated into Eq. (50) in Sec. IV by considering the proper multi-channel formalism, with the \tilde{G}_0^{-1} going over into the diagonal matrix of inverse propagators \hat{I} defined below Eq. (50). To sort out the prefactors, *cf.* Eq. (20) and note that \tilde{V} —via K as given in Eq. (A3)—contains a factor $(-i)$. Finally, upon S-wave projection of all quantities, the operator products (in momentum space) become

$$AB = \int \frac{d^3q}{(2\pi)^3} A(\dots, \mathbf{q})B(\mathbf{q}, \dots) \longrightarrow \frac{1}{2\pi^2} \int dq q^2 A(\dots, q)B(q, \dots), \quad (\text{A46})$$

which is exactly the operation “ \otimes ” that appears in Eq. (50).

Appendix B: Partially screened Coulomb T-matrix

In this section we discuss an approximate expression for the full off-shell Coulomb T-matrix with Yukawa (photon-mass) screening, based on results originally derived by Gorshkov in the 1960s [55, 56].

²⁰ Note the overall i in the prefactor in Eq. (9) and that remaining terms are real for $p_0 < 0$ and $\varepsilon \rightarrow 0$.

1. Unscreened Coulomb interaction

Closed expressions for the full off-shell Coulomb T-matrix have been known for a long time (see, for example, the review by Chen and Chen [60]). We consider here a quantum-mechanical two-particle system with reduced mass μ and charges $Z_{1,2}$. By writing the Coulomb interaction as an operator \hat{V}_C with

$$\langle \mathbf{r} | \hat{V}_C | \mathbf{r}' \rangle = \delta^{(3)}(\mathbf{r} - \mathbf{r}') V_C(\mathbf{r}) \quad \text{with} \quad V_C(\mathbf{r}) = V_C(r) \equiv \frac{\alpha Z_1 Z_2}{r}, \quad (\text{B1})$$

$$\langle \mathbf{p} | \hat{V}_C | \mathbf{q} \rangle = \frac{4\pi\alpha Z_1 Z_2}{(\mathbf{p} - \mathbf{q})^2} \equiv V_C(\mathbf{p}, \mathbf{q}), \quad (\text{B2})$$

the Lippmann-Schwinger equation for the Coulomb T-matrix T_C reads

$$\hat{T}_C(E) = \hat{V}_C + \hat{V}_C \hat{G}_0^{(+)}(E) \hat{T}_C(E), \quad (\text{B3})$$

where the energy E is a free (complex) parameter and

$$G_0^{(+)}(E; \mathbf{q}, \mathbf{q}') = \langle \mathbf{q} | \hat{G}_0^{(+)}(E) | \mathbf{q}' \rangle = \frac{(2\pi)^3 \delta^{(3)}(\mathbf{q} - \mathbf{q}')}{E - q^2/(2\mu) + i\epsilon}. \quad (\text{B4})$$

Introducing the (complex) momentum scale k via $E = k^2/(2\mu)$, the explicit solution of Eq. (B3) can be written in the Hostler form [60–62] as

$$T_C(k; \mathbf{p}, \mathbf{q}) = V_C(\mathbf{p}, \mathbf{q}) \left\{ 1 - 2i\eta \int_1^\infty \left(\frac{s+1}{s-1} \right)^{-i\eta} \frac{ds}{s^2 - 1 - \epsilon} \right\}, \quad (\text{B5})$$

where

$$\eta = \frac{\alpha\mu Z_1 Z_2}{k} \quad (\text{B6})$$

and

$$\epsilon = \frac{(p^2 - k^2)(q^2 - k^2)}{k^2(\mathbf{p} - \mathbf{q})^2}. \quad (\text{B7})$$

This integral representation is what is used to include Coulomb effects in the ^3He calculation of Ando and Birse [24]. Alternatively, it can be recast in terms of hypergeometric functions as

$$T_C(k; \mathbf{p}, \mathbf{q}) = V_C(\mathbf{p}, \mathbf{q}) \left\{ 1 - \Delta^{-1} \left[{}_2F_1 \left(1, i\eta, 1 + i\eta; \frac{\Delta - 1}{\Delta + 1} \right) - {}_2F_1 \left(1, i\eta, 1 + i\eta; \frac{\Delta + 1}{\Delta - 1} \right) \right] \right\}, \quad (\text{B8})$$

with the new variable Δ defined via

$$\Delta^2 = 1 + \epsilon. \quad (\text{B9})$$

2. Yukawa screening

As noted in Ref. [24], the unscreened Coulomb T-matrix certainly cannot be used in the scattering regime. We thus consider here an exponential (Yukawa) screening in configuration space,

$$V_C(\mathbf{r}) \longrightarrow V_{C,\lambda}(\mathbf{r}) = \alpha Z_1 Z_2 \frac{e^{-\lambda r}}{r}, \quad (\text{B10})$$

corresponding to the introduction of a photon mass λ in momentum space:

$$V_{C,\lambda}(\mathbf{p}, \mathbf{q}) = \frac{4\pi\alpha Z_1 Z_2}{(\mathbf{p} - \mathbf{q})^2 + \lambda^2}. \quad (\text{B11})$$

Ref. [60] gives an expression for what we in the following call the “partially screened” Coulomb T-matrix $\hat{T}_{C,\lambda}$, originally derived by Gorshkov [56]. It is defined by the relation

$$\hat{T}_{C,\lambda} = \hat{V}_{C,\lambda} + \hat{V}_{C,\lambda} \hat{G}_0^{(+)} \hat{T}_C, \quad (\text{B12})$$

where we have not written out the energy dependence to simplify the notation.

Note that Eq. (B12) is not a Lippmann–Schwinger equation because the operator that appears on the right-hand side is the unscreened Coulomb T-matrix \hat{T}_C . Still, $\hat{T}_{C,\lambda}$ is an interesting object to study because it can be written down as a closed expression that converges to the unscreened Coulomb T-matrix \hat{T}_C in the limit $\lambda \rightarrow 0$. Due to this property it should be useful in numerical calculations where one wants to include nonperturbative Coulomb effects in the scattering regime. Ideally, one would of course like to use an expression for the exact Yukawa T-matrix in such an approach, but no closed solution for that quantity is known so far. We thus propose to use $\hat{T}_{C,\lambda}$ as a pragmatic alternative. Since it has the right behavior in the limit $\lambda \rightarrow 0$, we expect it to adequately describe most of the nonperturbative Coulomb effects in that limit.

Unfortunately, the expression given for $T_{C,\lambda}(k; \mathbf{p}, \mathbf{q})$ in Eqs. (246) and (247) of Ref. [60] is not fully correct.²¹ Since in the original paper by Gorshkov [56] the limit $\lambda \rightarrow 0$ is taken without first giving the explicit form of the partially screened T-matrix, we will derive it here in the following.

To this end we start from Eq. (244) of Ref. [60], which in our notation reads

$$\begin{aligned} T_{C,\lambda}(k; \mathbf{p}, \mathbf{q}) &= V_{C,\lambda}(\mathbf{p}, \mathbf{q}) - i\eta \int_0^1 \frac{dx}{\Lambda_0(x)} V_{C,\lambda-ik\Lambda_0(x)}(x\mathbf{p}, \mathbf{q}) \times \exp \left\{ -i\eta \int_x^1 \frac{dx_1}{x_1 \Lambda_0(x_1)} \right\}, \quad (\text{B13}) \end{aligned}$$

with $\Lambda_0(x)$ defined as the positive root of

$$\Lambda_0^2(x) = [1 - (p/k)^2 x] (1 - x). \quad (\text{B14})$$

²¹ This can be seen by a straightforward dimensional analysis of Eq. (247) in Ref. [60]. Furthermore, the prefactor in Eq. (246) is written in terms of the unscreened Coulomb potential, which is clearly not correct.

$V_{C,\lambda-ik\Lambda_0(x)}$ is just the Yukawa potential (B11) with the substitution $\lambda \rightarrow \lambda - ik\Lambda_0(x)$. To simplify the integral in Eq. (B13) we write [56]

$$x = \frac{s^2 - 1}{s^2 - (p/k)^2}, \quad \frac{dx}{ds} = \frac{2s(1 - (p/k)^2)}{(s^2 - (p/k)^2)^2} \quad (\text{B15})$$

and find that

$$\Lambda_0(x) = s(1 - x). \quad (\text{B16})$$

Since furthermore

$$1 - x = \frac{1 - (p/k)^2}{s^2 - (p/k)^2}, \quad (\text{B17})$$

the integral in the exponent is just

$$\int_x^1 \frac{dx_1}{x_1 \Lambda_0(x_1)} = \int_s^\infty \frac{2 ds_1}{s_1^2 - 1} = \log\left(\frac{s+1}{s-1}\right). \quad (\text{B18})$$

For the potential term under the integral we get

$$V_{C,\lambda-ik\Lambda_0(x)}(x\mathbf{p}, \mathbf{q}) = \frac{2\pi\gamma}{\mu} \times \frac{(s^2 - (p/k)^2)}{(s^2 - 1)(\mathbf{q} - \mathbf{p})^2 + \frac{1}{k^2} \left[\lambda^2(k^2 s^2 - p^2) - 2i\lambda k s(k^2 - p^2) - (k^2 - q^2)(k^2 - p^2) \right]} \quad (\text{B19})$$

after a lengthy but straightforward calculation. Adding

$$0 = \lambda^2(s^2 - 1) - \lambda^2 s^2 + \lambda^2 \quad (\text{B20})$$

in the denominator, we can rewrite this as

$$V_{C,\lambda-ik\Lambda_0(x)}(x\mathbf{p}, \mathbf{q}) = \frac{2\pi\gamma}{\mu} \times \frac{(s^2 - (p/k)^2)}{(s^2 - 1)[(\mathbf{q} - \mathbf{p})^2 + \lambda^2] - \frac{1}{k^2} [(k^2 - q^2)(k^2 - p^2)] + \frac{1}{k^2} [(k^2 - p^2)(\lambda^2 - 2i\lambda k s)]}. \quad (\text{B21})$$

Finally, noting that the term in the numerator cancels against the same factor in

$$\frac{dx}{\Lambda_0(x)} = \frac{2 ds}{s^2 - (p/k)^2}, \quad (\text{B22})$$

and factoring out the Yukawa potential, we arrive at

$$T_{C,\lambda}(k; \mathbf{p}, \mathbf{q}) = V_{C,\lambda}(\mathbf{p}, \mathbf{q}) \left\{ 1 - 2i\eta \int_1^\infty \left(\frac{s+1}{s-1}\right)^{-i\eta} \frac{ds}{s^2 - 1 - \epsilon_\lambda + \zeta_\lambda(s)} \right\} \quad (\text{B23})$$

with

$$\epsilon_\lambda = \frac{(k^2 - p^2)(k^2 - q^2)}{k^2 [(\mathbf{q} - \mathbf{p})^2 + \lambda^2]} \quad (\text{B24})$$

and

$$\zeta_\lambda(s) = \frac{(k^2 - p^2)(\lambda^2 - 2i\lambda ks)}{k^2 [(\mathbf{q} - \mathbf{p})^2 + \lambda^2]}. \quad (\text{B25})$$

This expression is very similar to the integral form of the unscreened Coulomb T-matrix. The only differences are given by the new term $\zeta_\lambda(s)$ in the denominator and the fact that all singularities, both in the overall prefactor and under the integral, are now regulated by adding λ^2 . In fact, one directly sees that in the limit $\lambda \rightarrow 0$, Eq. (B23) converges to the unscreened expression given in Eq. (B5).

3. Expression in terms of hypergeometric functions

Something that is not noted in Refs. [60] and [56] is that—just like the unscreened Coulomb T-matrix— $T_{C,\lambda}(k; \mathbf{p}, \mathbf{q})$ can also be expressed in terms of hypergeometric functions. To obtain this expression we first note that the denominator in Eq. (B23) can be written as

$$s^2 - 1 - \epsilon_\lambda + \zeta_\lambda(s) = s^2 - (1 + d_1 \cdot D^2) - (d_2 \cdot D^2)s \quad (\text{B26})$$

with

$$d_1 = k^2 - q^2 - \lambda^2, \quad d_2 = 2i\lambda k \quad (\text{B27})$$

and

$$D^2 = \frac{k^2 - p^2}{k^2 [(\mathbf{q} - \mathbf{p})^2 + \lambda^2]}. \quad (\text{B28})$$

After making the transformation

$$s = \frac{t+1}{t-1}, \quad \int_1^\infty ds = 2 \int_1^\infty \frac{dt}{(t-1)^2} \quad (\text{B29})$$

we get

$$T_{C,\lambda}(k; \mathbf{p}, \mathbf{q}) = V_{C,\lambda}(\mathbf{p}, \mathbf{q}) \times \left\{ 1 - 4i\eta \int_1^\infty \frac{t^{-i\eta} dt}{-D^2(d_1 + d_2)t^2 + (4 + 2D^2 \cdot d_1)t - D^2(d_1 - d_2)} \right\}. \quad (\text{B30})$$

To proceed further, we use the indefinite integral²²

$$\int \frac{t^\nu dt}{x_2 t^2 + x_1 t + x_0} = \frac{1}{X_1} \frac{2^{-\nu} t^\nu}{\nu} \left\{ {}_2F_1(-\nu, -\nu; 1 - \nu; X_2^+(t)) \cdot X_3^+(t)^{-\nu} - {}_2F_1(-\nu, -\nu; 1 - \nu; X_2^-(t)) \cdot X_3^-(t)^{-\nu} \right\}, \quad (\text{B31})$$

where

$$X_1 = \sqrt{x_1^2 - 4x_0x_2}, \quad X_2^\pm(t) = \frac{x_1 \mp X_1}{x_1 + 2tx_2 \mp X_1}, \quad X_3^\pm(t) = \frac{tx_2}{x_1 + 2tx_2 \mp X_1}. \quad (\text{B32})$$

²² This result has been obtained with the help of a computer algebra software (Wolfram Mathematica).

Evaluating this at $t = 1$ is straightforward, but considering $t \rightarrow \infty$ requires a little more care. From Eq. (B32) one sees that $X_2^\pm(t)$ goes to zero like $1/t$ as $t \rightarrow \infty$, such that the hypergeometric functions simply yield one in this limit. Since the potentially problematic (because $\nu = -i\eta$) prefactor t^ν is cancelled by the numerator of $X_3^\pm(t)^{-\nu}$ with the remainder then going to zero as $t \rightarrow \infty$, we can conclude that there is actually no contribution to the integral from the upper boundary in Eq. (B30) and that its value is hence given by the right-hand side of Eq. (B31) with $t = 1$.

Before inserting this into Eq. (B30), we subsequently apply the identities [63]

$${}_2F_1(a, b; c; z) = (1 - z)^{c-a-b} {}_2F_1(c - a, c - b; c; z) \quad (\text{B33})$$

and

$${}_2F_1(a, b; c; z) = (1 - z)^{-a} {}_2F_1\left(a, c - b; c; \frac{z}{z - 1}\right) \quad (\text{B34})$$

to rewrite

$$\begin{aligned} {}_2F_1(-\nu, -\nu; 1 - \nu; z) &= (1 - z)^{1+\nu} {}_2F_1(1, 1; 1 - \nu; z) \\ &= (1 - z)^\nu {}_2F_1\left(1, -\nu; 1 - \nu; \frac{z}{z - 1}\right). \end{aligned} \quad (\text{B35})$$

This is useful because from Eq (B32) one finds that for $z = X_2^\pm(t)$,

$$(1 - z)^\nu = 2^\nu X_3^\pm(t)^\nu, \quad (\text{B36})$$

canceling the inverse factors of this in Eq. (B31). Moreover, the arguments simplify to

$$\frac{z}{z - 1} = -\frac{1}{2} \frac{X_2^\pm(t)}{X_3^\pm(t)} = -\frac{x_1 \mp X_1}{2t x_2}. \quad (\text{B37})$$

With this, we then have

$$\begin{aligned} \int_1^\infty \frac{t^\nu dt}{x_2 t^2 + x_1 t + x_0} &= \frac{1}{\nu X_1} \left\{ {}_2F_1\left(1, -\nu; 1 - \nu; -\frac{x_1 + X_1}{2x_2}\right) \right. \\ &\quad \left. - {}_2F_1\left(1, -\nu; 1 - \nu; -\frac{x_1 - X_1}{2x_2}\right) \right\}. \end{aligned} \quad (\text{B38})$$

Finally, applying the above result to Eq. (B30), we can write the partially-screened Coulomb T-matrix as

$$\begin{aligned} T_{C,\lambda}(k; \mathbf{p}, \mathbf{q}) &= V_C(\mathbf{p}, \mathbf{q}) \left\{ 1 - \Delta_\lambda^{-1} [{}_2F_1(1, i\eta, 1 + i\eta; X_\lambda^-) - {}_2F_1(1, i\eta, 1 + i\eta; X_\lambda^+)] \right\}, \end{aligned} \quad (\text{B39})$$

with

$$\Delta_\lambda^2 = 1 + \frac{(k^2 - p^2)(k^2 - q^2 - \lambda^2)}{k^2 [(\mathbf{q} - \mathbf{p})^2 + \lambda^2]} - \frac{\lambda^2(k^2 - p^2)^2}{k^2 [(\mathbf{q} - \mathbf{p})^2 + \lambda^2]^2} \quad (\text{B40})$$

and

$$X_{\lambda}^{\pm} = \frac{2k^2 [(\mathbf{q} - \mathbf{p})^2 + \lambda^2] (1 \pm \Delta_{\lambda}) + (k^2 - p^2)(k^2 - q^2 - \lambda^2)}{(k^2 - p^2) [(k + i\lambda)^2 - q^2]}. \quad (\text{B41})$$

As it should, this reduces to the hypergeometric expression (B8) for the unscreened Coulomb T-matrix in the limit $\lambda \rightarrow 0$. It is directly clear from Eqs. (B40) and (B9) that

$$\lim_{\lambda \rightarrow 0} \Delta_{\lambda}^2 = \Delta^2, \quad (\text{B42})$$

and a straightforward calculation then furthermore shows that

$$\lim_{\lambda \rightarrow 0} X_{\lambda}^{\pm} = \frac{\Delta \pm 1}{\Delta \mp 1}. \quad (\text{B43})$$

-
- [1] D. B. Kaplan, M. J. Savage and M. B. Wise, Nucl. Phys. B **534**, (1998) 329 [arXiv:nucl-th/9802075].
 - [2] U. van Kolck, Nucl. Phys. A **645**, (1999) 273 [arXiv:nucl-th/9808007].
 - [3] J. -W. Chen, G. Rupak and M. J. Savage, Nucl. Phys. A **653** (1999) 386 [nucl-th/9902056].
 - [4] H. A. Bethe, Phys. Rev. **76** (1949) 38.
 - [5] V. Efimov, Nucl. Phys. A **362** (1981) 45.
 - [6] H.-W. Hammer and L. Platter, Ann. Rev. Nucl. Part. Sci. **60** (2010) 207 [arXiv:1001.1981 [nucl-th]].
 - [7] J. J. de Swart, C. P. F. Terheggen and V. G. J. Stoks, arXiv:nucl-th/9509032.
 - [8] S. R. Beane, P. F. Bedaque, W. C. Haxton, D. R. Phillips and M. J. Savage, arXiv:nucl-th/0008064.
 - [9] P. F. Bedaque and U. van Kolck, Phys. Lett. B **428** (1998) 221 [nucl-th/9710073].
 - [10] P. F. Bedaque, H. W. Hammer and U. van Kolck, Phys. Rev. C **58** (1998) 641 [nucl-th/9802057].
 - [11] P. F. Bedaque, H.-W. Hammer and U. van Kolck, Nucl. Phys. A **676** (2000) 357 [arXiv:nucl-th/9906032].
 - [12] F. Gabbiani, P. F. Bedaque and H. W. Griebhammer, Nucl. Phys. A **675** (2000) 601 [arXiv:nucl-th/9911034].
 - [13] H. W. Hammer and T. Mehen, Phys. Lett. B **516**, 353 (2001) [nucl-th/0105072].
 - [14] P. F. Bedaque, G. Rupak, H. W. Griebhammer and H.-W. Hammer, Nucl. Phys. A **714** (2003) 589 [arXiv:nucl-th/0207034].
 - [15] J. Vanasse, Phys. Rev. C **88** (2013) 044001 [arXiv:1305.0283 [nucl-th]].
 - [16] X. Kong and F. Ravndal, Phys. Lett. B **450** (1999) 320 [arXiv:nucl-th/9811076].
 - [17] X. Kong and F. Ravndal, Nucl. Phys. A **665** (2000) 137 [arXiv:hep-ph/9903523].
 - [18] S.-I. Ando, J. W. Shin, C. H. Hyun and S. W. Hong, Phys. Rev. C **76** (2007) 064001 [arXiv:0704.2312 [nucl-th]].
 - [19] T. Barford and M. C. Birse, Phys. Rev. C **67** (2003) 064006 [arXiv:hep-ph/0206146].
 - [20] S.-I. Ando and M. C. Birse, Phys. Rev. C **78** (2008) 024004 [arXiv:0805.3655 [nucl-th]].
 - [21] X. Kong and F. Ravndal, Phys. Rev. C **64** (2001) 044002 [arXiv:nucl-th/0004038].
 - [22] S.-I. Ando, J. W. Shin, C. H. Hyun, S. W. Hong and K. Kubodera, Phys. Lett. B **668** (2008) 187 [arXiv:0801.4330 [nucl-th]].

- [23] G. Rupak and X. Kong, Nucl. Phys. A **717** (2003) 73 [arXiv:nucl-th/0108059].
- [24] S. Ando and M. C. Birse, J. Phys. G: Nucl. Part. Phys. **37** (2010) 105108 [arXiv:1003.4383 [nucl-th]].
- [25] J. Kirscher, H. W. Griebhammer, D. Shukla and H. M. Hofmann, Eur. Phys. J. A **44** (2010) 239 [arXiv:0903.5538 [nucl-th]].
- [26] S. König and H.-W. Hammer, Phys. Rev. C **83** (2011) 064001 [arXiv:1101.5939 [nucl-th]].
- [27] S. König, *Effective quantum theories with short- and long-range forces*, Doctorial thesis (Dissertation), University of Bonn, 2013.
- [28] J. Vanasse, D. A. Egolf, J. Kerin, S. König and R. P. Springer, Phys. Rev. C **89** (2014) 6, 064003 [arXiv:1402.5441 [nucl-th]].
- [29] D. B. Kaplan, Nucl. Phys. B **494** (1997) 471 [nucl-th/9610052].
- [30] P. F. Bedaque and H. W. Griebhammer, Nucl. Phys. A **671** (2000) 357.
- [31] D. R. Phillips and T. D. Cohen, Phys. Lett. B **390** (1997) 7 [arXiv:nucl-th/9607048].
- [32] H.-W. Hammer and D. Lee, Phys. Lett. B **681** (2009) 500 [arXiv:0907.1763 [nucl-th]].
- [33] H.-W. Hammer and D. Lee, Annals Phys. **325** (2010) 2212 [arXiv:1002.4603 [nucl-th]].
- [34] J. Kirscher and D. R. Phillips, Phys. Rev. C **84** (2011) 054004 [arXiv:1106.3171 [nucl-th]].
- [35] H. W. Griebhammer, M. R. Schindler and R. P. Springer, Eur. Phys. J. A **48** (2012) 7 [arXiv:1109.5667 [nucl-th]].
- [36] D. B. Kaplan, M. J. Savage and M. B. Wise, Phys. Lett. B **424** (1998) 390 [nucl-th/9801034].
- [37] D. R. Phillips, G. Rupak and M. J. Savage, Phys. Lett. B **473** (2000) 209 [nucl-th/9908054].
- [38] H. W. Griebhammer, Nucl. Phys. A **744** (2004) 192 [nucl-th/0404073].
- [39] C. Ji and D. R. Phillips, Few-Body Syst. **54** (2013) 2317 [arXiv:1212.1845 [nucl-th]].
- [40] S. König and H.-W. Hammer, Phys. Rev. C **90** (2014) 3, 034005 [arXiv:1312.2573 [nucl-th]].
- [41] S. König, D. Lee and H. -W. Hammer, J. Phys. G: Nucl. Part. Phys. **40** (2013) 045106 [arXiv:1210.8304 [nucl-th]].
- [42] P. F. Bedaque and U. van Kolck, Ann. Rev. Nucl. Part. Sci. **52** (2002) 339 [arXiv:nucl-th/0203055].
- [43] E. Epelbaum, H.-W. Hammer and U.-G. Meißner, Rev. Mod. Phys. **81** (2009) 1773 [arXiv:0811.1338 [nucl-th]].
- [44] M. Walzl, U. G. Meißner and E. Epelbaum, Nucl. Phys. A **693** (2001) 663 [nucl-th/0010019].
- [45] H. W. Griebhammer, Nucl. Phys. A **760** (2005) 110 [arXiv:nucl-th/0502039].
- [46] C. van der Leun and C. Anderjaska, Nucl. Phys. A **380** (1982), 261.
- [47] M. A. Preston and R. K. Bhaduri, *Structure of the Nucleus*, Addison-Wesley Publishing Company, Reading, MA (1975).
- [48] J. R. Bergervoet, P. C. van Campen, W. A. van der Sanden and J. J. de Swart, Phys. Rev. C **38** (1988) 15.
- [49] V. K. Agrawala, J. G. Belinfante, and G. H. Renninger, Nuov. Cim. A **44** (1966) 740.
- [50] P. Hagen, H.-W. Hammer and L. Platter, Eur. Phys. J. A **49** (2013) 118 [arXiv:1304.6516 [nucl-th]].
- [51] L. P. Kok, D. J. Struik, and H. van Haeringen, Internal Report 151 (1979), University of Groningen.
- [52] L. P. Kok, D. J. Struik, J. E. Holwerda, and H. van Haeringen, Internal Report 170 (1979), University of Groningen.
- [53] M. Hoferichter, *Private communication* (2010).
- [54] L. Platter, D. R. Phillips, Few Body Syst. **40** (2006) 35 [arXiv:cond-mat/0604255].
- [55] V. G. Gorshkov, Sov. Phys. JETP **13** (1961) 1037.

- [56] V. G. Gorshkov, Sov. Phys. JETP **20** (1965) 234.
- [57] T. Hahn, Comput. Phys. Commun. **168** (2005) 78 [hep-ph/0404043]
<http://www.feynarts.de/cuba/>.
- [58] N. Michel and M.V. Stoitsov, Comput. Phys. Comm. **178** (2008) 535.
<http://cpc.cs.qub.ac.uk/cpc/>, Catalogue ID “AEAE”
- [59] D. Lurie, *Particles and Fields*, Interscience Publishers (1968).
- [60] J. C. Y. Chen and A. C. Chen, Adv. Atom. Mol. Phys. **8** (1972) 72.
- [61] L. Hostler, J. Math. Phys. **5** (1964) 591.
- [62] L. Hostler, J. Math. Phys. **5** (1964) 1235.
- [63] M. Abramowitz and I. A. Stegun, *Pocketbook of Mathematical Functions*, Verlag Harri Deutsch, Thun; Frankfurt am Main (1984).